Geochimica et Cosmochimica Acta 410 (2025) 174–187

Contents lists available at ScienceDirect

Geochimica et Cosmochimica Acta

journal homepage: www.elsevier.com/locate/gca

Most bivalves and gastropods calcify indistinguishably from dual clumped isotope equilibrium

Vanessa Schlidt [a,*], David Evans [a,b], Niels J. de Winter [c], Miguel Bernecker [a], Iris Arndt [a], Philip T. Staudigel [a], Amelia J. Davies [a,d], Uwe Brand [e], Wolfgang Müller [a], Jens Fiebig [a,*]

[a] Institute of Geosciences, Goethe University Frankfurt, Altenhöferallee 1, 60438 Frankfurt am Main, Germany
[b] School of Ocean and Earth Science, University of Southampton, Southampton, United Kingdom
[c] Department of Earth Sciences, Vrije Universiteit Amsterdam, the Netherlands
[d] Institute for Geology and Mineralogy, University of Cologne, Cologne, Germany
[e] Department of Earth Sciences, Brock University, St. Catharines, Ontario, Canada

ARTICLE INFO

Associate editor: Benjamin H. Passey

Keywords:
Carbonate clumped isotopes
Molluscs
Biomineralisation
Paleoclimate

ABSTRACT

Molluscan shell-carbonates are extensively used to reconstruct paleo-temperatures at sub-annual resolution. The accurate application of two widely used temperature proxies, the shell carbonate oxygen isotope ($\delta^{18}O$) and carbonate clumped isotope (Δ_{47}) composition, is based on the assumption that kinetic processes in the DIC-H_2O-$CaCO_3$ system were either absent or invariant during shell formation, and thus can be corrected for using empirical calibrations.

Here, we analysed the dual clumped isotope composition, Δ_{47} and Δ_{48}, of a wide range of modern and Eocene molluscs (bivalves and gastropods) to investigate the potential importance of kinetics during molluscan biomineralisation. We show that Δ_{47} and Δ_{48} values of most of our modern samples are indistinguishable from equilibrium. For these samples, Δ_{47}-derived temperatures conform to corresponding growth temperatures within their fully propagated 95 % uncertainties of $\leq \pm 2.3$ °C. Significant departures from equilibrium values are only observed for a single gastropod specimen characterised by a growth temperature < 10 °C. Together, these results strongly imply that bivalve and gastropod shell carbonate archives can be used for accurate and highly precise reconstructions of sea surface temperatures by means of clumped isotope thermometry. Kinetic biases on this thermometer, if relevant at all, may only become important at relatively low temperatures.

Δ_{47}-derived temperatures for our Eocene samples (~39 Ma) from the Hampshire Basin (paleo-latitude ~ 40°N) range from 17.3 to 23.2 °C. These paleo-temperatures are in agreement with sea surface temperatures for mid-Eocene mid latitude regions based on foraminifera clumped isotopes; adding confidence to both datasets. In order to aid the accurate reconstruction of seawater $\delta^{18}O$ values, we compiled published oxygen isotope fractionation data for molluscs and established relationships that describe the temperature dependence of oxygen isotope fractionation between water and molluscan calcite and aragonite, respectively. Applying the equation for aragonite to the Eocene samples, we obtain reconstructed seawater $\delta^{18}O$ values for the Hampshire Basin between −2.2 and −3.4 ‰ (VSMOW), similarly in agreement with previous approaches suggesting a freshwater-influenced surface ocean composition in this region.

1. Introduction

Accurate reconstruction of Earth's surface temperatures during periods of elevated atmospheric CO_2 levels is of great importance for testing the skill of climate models that are used to predict future climate change. To accomplish this task, it is necessary to identify geochemical proxies and sedimentary archives that reliably record Earth's surface temperatures in deep time. This is important, because the most recent time interval characterised by a global climate state similar to the worst-case end-of-century CO_2 predictions occurred millions of years ago (e.g., Judd et al., 2024).

Molluscan shells represent an archive that enables climate reconstruction across such an extent of geological time. Molluscs make up one of the most diverse groups of calcifying organisms on Earth, inhabiting a

* Corresponding authors.
E-mail addresses: schlidt@em.uni-frankfurt.de (V. Schlidt), Jens.Fiebig@em.uni-frankfurt.de (J. Fiebig).

https://doi.org/10.1016/j.gca.2025.10.008
Received 3 March 2025; Accepted 7 October 2025
Available online 11 October 2025

wide range of terrestrial and marine habitats. Their (continuous) occurrence in the fossil record reaches back as far as the early Cambrian (e.g., Immenhauser et al., 2016 and references therein), and they achieved dominance in abundance over brachiopods by the end of the Permian (Payne et al., 2014). Molluscs form shells of calcite, aragonite, and sometimes high-Mg calcite and vaterite (Nehrke et al., 2012), or combinations thereof. Mollusc-based paleo-temperature reconstructions have predominantly utilised the oxygen isotope composition ($\delta^{18}O$) of their shells (e.g., Schöne et al., 2005; Butler et al., 2015; Huyghe et al., 2015; de Winter et al., 2020, Ivany et al., 2022; Arndt et al., 2024), requiring the oxygen isotope composition of seawater to be known or assumed.

The carbonate clumped isotope thermometer (Ghosh et al., 2006) avoids this issue as it is based on the temperature dependence of the Δ_{47} value. This value compares the abundance of ^{13}C-^{18}O-bearing isotopologues in the CO_2 derived from phosphoric acid digestion of carbonates with its stochastically predicted abundance (Ghosh et al., 2006), which is independent of the oxygen isotope composition of seawater. Nonetheless, the attainment of homogeneous isotopic equilibrium in the solution from which $CaCO_3$ is precipitated (i.e., the isotopic equilibration between water and the DIC species) is a requirement for accurate temperature reconstructions using the Δ_{47}-thermometer. However, recent studies have revealed that many biogenic carbonates (e.g., corals, brachiopods, echinoids, and cephalopods) or inorganic carbonates (e.g., speleothems) record Δ_{47} signatures that are affected by kinetics (Affek, et al., 2014; Affek & Zaarur, 2014; Bajnai et al., 2018, 2020; Daeron et al., 2011; Davies & John, 2019; Davies et al., 2021; Guo, 2020; Guo & Zhou, 2019; Saenger et al., 2012, 2017).

The rate-limiting process in the equilibration of both clumped and oxygen isotopes within the DIC-H_2O-$CaCO_3$ system is the interconversion of aqueous CO_2 and HCO_3^- via (de)hydration and (de)hydroxylation reactions. If the precipitation rate of carbonate outpaces the equilibration rate of the DIC pool, the disequilibrium isotopic signatures present in the DIC pool will be inherited by the forming mineral (e.g., Watkins et al., 2013, 2014; Guo & Zhou, 2019). The direction and magnitude of these kinetic biases is governed by processes, such as addition or removal of CO_2, which can perturb the state of DIC during mineral formation (Guo, 2020). Since both the oxygen and clumped isotope composition of a carbonate follow the same chemical exchange reactions, $\delta^{18}O_{carb}$ and Δ_{47} can be used in conjunction to detect potential kinetic biases (e.g., Bajnai et al., 2018). However, the uncertainties introduced by the absence of knowledge of paleo-water $\delta^{18}O$ values impairs the application of paired $\delta^{18}O_{carb}$ and Δ_{47} measurements for diagnosing kinetic biases in fossil archives. The presence of kinetic biases in carbonate formation temperatures derived from oxygen isotope and Δ_{47} thermometry may be overcome by applying species-specific temperature calibrations (e.g., Weber & Woodhead, 1972; McConnaughey et al., 1989a; Davies et al., 2023) provided disequilibrium offsets are invariant through space and time.

The addition of a second thermodynamically controlled metric that is independent of fluid-$\delta^{18}O$ has become possible through high-precision Δ_{48} analysis, which addresses measured and stochastic abundances of m/z 48 isotopologues (mainly $^{12}C^{18}O_2$) in the CO_2 evolved from phosphoric acid digestion of carbonates (Fiebig et al., 2019). Changes in Δ_{47} and Δ_{48} values and their precursors in the carbonate, Δ_{63} and Δ_{64}, respectively, are controlled by the same chemical processes. The simultaneous measurement of both Δ_{47} and Δ_{48} by dual clumped isotope analysis, allows isotopic disequilibrium signatures to be identified, and the extent of disequilibrium to be assessed. It also enables the identification of the underlying process through which carbonate precipitation was initiated by comparing measured dual clumped isotope data with the position of Δ_{47}-Δ_{48}-equilibrium (e.g., Bajnai et al., 2020; Fiebig et al., 2021). For example, if supersaturation and precipitation is concurrent with CO_2 absorption, as is the case in corals (e.g., Thiagarajan et al., 2011; Saenger et al., 2012; Spooner et al., 2016) kinetic limitation will be expressed in positive Δ_{47} and negative Δ_{48} offsets from equilibrium (Guo, 2020; Bajnai et al., 2020). If, on the contrary, supersaturation and precipitation is accompanied with or driven by net CO_2 degassing, as is characteristic for speleothems, kinetic limitation evokes $-\Delta_{47}/+\Delta_{48}$ disequilibrium patterns (Guo & Zhou, 2019; Guo, 2020; Bajnai et al., 2020). Since its invention, dual clumped isotope thermometry has been used to identify kinetic bias in cold and warm water corals (Davies et al., 2022), brachiopods (Davies et al., 2023), bird eggshells (Tagliavento et al., 2023), speleothems (Bajnai et al., 2020; Parvez et al., 2024), authigenic methane seep carbonates (Staudigel et al., 2024), freshwater cements (Lu et al., 2024), microbial carbonates (Ingalls et al., 2024; Lu & Swart, 2024), and in carbonates associated with the serpentinisation of ultramafic rocks (Parvez et al., 2023). Crucially, it has been shown that kinetic biases in corals, brachiopods, speleothems and methane seep carbonates follow identifiable model-predicted disequilibrium trajectories. These can be used to correct measured dual clumped isotope data and, finally, to isolate the temperature signal recorded in the carbonate. If, on the contrary, kinetic biases remain undetected, and no empirical calibration is available for an archive of interest that accounts for this kinetic bias, these would result in erroneous growth temperature reconstructions from measured Δ_{47} values. Such reconstructed growth temperatures would be overestimated or underestimated if CO_2 removal or CO_2 absorption, respectively, were rate-limiting.

Previous investigations revealed that kinetic biases in Δ_{47} values of mollusc shells, if present at all, might only be weakly pronounced. Huyghe et al. (2022) and de Winter et al. (2022) analysed shells of marine bivalves and oysters grown at temperatures of −2 to 27 °C. With the exception of juvenile oysters, Δ_{47} values obtained by Huyghe et al. (2022) agreed with those predicted by the unified calibration of Anderson et al. (2021) which, in turn, is indistinguishable from the inorganic calcite equilibrium Δ_{47}-T relationship of Fiebig et al. (2021). On the contrary, formation temperatures for *A. islandica* were slightly, but significantly (2.7 ± 2.0 °C) underestimated by de Winter et al. (2022) who also projected Δ_{47} values to the Anderson et al. (2021) relationship. Curley et al. (2023) investigated fossil bivalves of unconstrained growth temperatures. Based on intra-shell alignments between Δ_{47} and $\delta^{18}O_{carb}$ they postulated that the inner shell layer is prone to kinetic isotope effects, whereas the outer shell layer is not.

In this study, we analysed the dual clumped isotope composition of twelve modern and five fossil mollusc species for a total of 21 specimens to investigate whether their clumped isotope composition is affected by rate-limiting kinetics. We demonstrate that most of our sampled shells calcify indistinguishably from dual clumped isotope equilibrium which makes bivalves and gastropods excellent archives for high-precision paleo-temperature reconstructions using Δ_{47}-thermometry, especially at moderate to warm temperatures. We also compile mollusc-specific aragonite and calcite oxygen isotope data in order to refine the 1000lnα($CaCO_3$-H_2O)-T relationships. Finally, we apply the dual clumped isotope thermometer to five Eocene molluscs from the Hampshire Basin, reconstruct sea surface temperatures and seawater-$\delta^{18}O$, and compare these estimates to data previously reconstructed for the same geographic region and age.

2. Material and methods

We analysed twenty-one molluscan samples for their dual clumped and bulk stable isotope compositions, consisting of sixteen modern and five specimens from the mid Eocene (Bartonian; ~39 Ma). Metadata for all samples are listed in Table 1.

2.1. Modern samples

Names and details of modern specimens measured in this study are provided in Table 1. Independently constrained growth temperatures and independently constrained $\delta^{18}O_{SW}$ values of these samples are listed in Table 2.

Table 1
Metadata for the investigated mollusc samples.

Sample	Species	Origin	Sampled part	Mineralogy
RG1	*Buccinum undatum* LINNAEUS 1758	Fife, Scotland, UK	Whole shell	Ar
RG2	*Patella vulgata* LINNAEUS 1758	Fife, Scotland, UK	Whole shell	Cc (>80 %) Ar
RG2_U	*Patella vulgata* LINNAEUS 1758	Fife, Scotland, UK	Subsample RG2, no oxidative cleaning	Cc (>80 %) Ar
RM1	*Modiolus modiolus* (LINNAEUS 1758)	Fife, Scotland, UK	Whole shell	Ar
RM2	*Spisula solida* (LINNAEUS 1758)	Fife, Scotland, UK	Whole shell	Ar
AL_006	*Arctica islandica* (LINNAEUS 1767)	Grown in culture (NIOZ), NL	Bulk sample	Ar
CHA_M_050	*Arctica islandica* (LINNAEUS 1767)	Dredged from NE coast of Iceland	Bulk sample (dual clumped data in Staudigel et al. (2023a)	Ar
CHA_M_062	*Arctica islandica* (LINNAEUS 1767)	Dredged from NE coast of Iceland	Bulk sample (dual clumped data in Staudigel et al. (2023a)	Ar
M2-Sf	*Magallana gigas* (THUNBERG 1793)	Mokbaai, Texel, NL	Seasonally averaged, entire hinge, foliated microstructure Geochemical data in de Winter et al. (2021a)	Cc
M2Sv	*Magallana gigas* (THUNBERG 1793)	Mokbaai, Texel, NL	Seasonally averaged, 2nd growth year Geochemical data in de Winter et al. (2021a)	Cc
ME_002	*Mytilus edulis* LINNAEUS 1758	Grown in culture (NIOZ), Grevelingen, NL	Bulk sample, Respiration rate data in Jansen et al. (2007)	Cc + Ar
ME_003	*Mytilus edulis* LINNAEUS 1758	Grown in culture (NIOZ), Grevelingen, NL	Bulk sample, Respiration rate data in Jansen et al. (2007)	Cc + Ar
Shell UC	*Hippopus porcellanus* ROSEWATER 1982	Antique trade	Along growth lines (Nooitgedacht et al., 2021)	Ar
Shell UH	*Hippopus porcellanus* ROSEWATER 1982	Antique trade	Along growth lines (Nooitgedacht et al., 2021)	Ar
TS2	*Tridacna Squamosa* LAMARCK 1819	Aquarium, Royal Burgers' Zoo, Amden, NL	Part of the inner shell	Ar
WS2	*Hiatella arctica* (LINNAEUS 1767)	White Sea, RU	Avoiding areas of muscle attachment and hinge	Ar
WS3	*Tridonta borealis* (*Astarte borealis*) (SCHUMACHER 1817)	White Sea, RU	Avoiding areas of muscle attachment and hinge	Ar
FG1	*Sycostoma* sp. COX 1931	Barton on Sea, England, UK	Whole shell	Ar
FG2	*Turricula (Orthosurcula) rostrata* (SOLANDER 1766)	Barton on Sea, England, UK	Whole shell	Ar
FG3	*Strombus athleta* (SOLANDER 1766)	Barton at Sea, England, UK	Whole shell	Ar
FM1	*Bathytormus sulcata* (SOLANDER 1766)	Barton at Sea, England, UK	Whole shell	Ar
FM2	*Arcturellina pusilla* (DESHAYES 1858)	Barton at Sea, England, UK	Whole shell	Ar

*NIOZ: Koninklijk Nederlands Instituut voor Onderzoek der Zee.

The bivalves *Modiolus modiolus* (RM1) and *Spisula solida* (RM2) as well as the gastropods *Buccinum undatum* (RG1) and *Patella vulgata* (RG2) were collected at low tide from a beach in southeast Scotland (Tentsmuir Forest) in March 2020. The average annual sea surface temperature for the site of sample collection is 9.6 °C determined using the World Ocean Atlas (WOA) 2023 (Locarnini et al., 2024), with a seasonal range of 7.0–12.4 °C. The oxygen isotope composition of seawater at the site of sample collection ($\delta^{18}O_{sw}$ = 0.2 ‰, VSMOW) was calculated based on gridded data provided by Harwood et al. (2008).

Some material for this study came from a population of cultured bivalves: *Arctica islandica* (AL_006) and *Mytilus edulis* (ME_002, ME_003) grew in culture at NIOZ (Royal Netherlands Institute for Sea Research). Growth temperatures for bivalves ME_002 and ME_003 range between 5 and 25 °C (seasonal temperature changes were imposed) with an average temperature of 16.2 °C during the culturing period. Bivalve AL_006 was cultured at a constant temperature of 12.0 °C.

M2-Sf and M2-Sv are sample powders from a cultured *Magellana gigas* (cf. *Crassostreas gigas*) specimen (additional geochemical data published in de Winter et al., 2021a). The imposed seasonal range of temperature for bivalves M2-Sf and M2-Sv varies between 4 and 19 °C with a mean of 11.5 °C. Reconstructed $\delta^{18}O_{sw}$ (VSMOW) is −1.55 ‰ (de Winter et al., 2021a). CHA_M_050 and CHA_M_062 are *A. islandica* specimens collected off the coast of NE Iceland (Pederson et al., 2019). The WOA2023-derived annual mean growth temperature (Locarnini et al., 2024) is 3.9 °C, while summer temperatures reach 7.4 °C. Dual clumped isotope data on these two samples has already been reported but discussed in a different context by Staudigel et al. (2023a). Bivalves Shell UC and Shell UH are *Hippopus porcellanus* specimens purchased at an antique trade; growth temperature and $\delta^{18}O$ values of the water are therefore unknown, although their growth temperatures can be estimated because *H. porcellanus* has a narrow distribution in the modern ocean. Specifically, this species mainly occurs around Indonesia, Palau, and the Philippines for which the WOA2023 (Locarnini et al., 2024) mean annual SST range is 27–31 °C. *Hyatella arctica* (WS2) and *Tridonta borealis* (WS3) originate from the White Sea (Barents Sea) which, at the site of collection, is characterised by a mean annual SST of 7.1 °C (seasonal range 0.3–13 °C) (WOA2023; Locarnini et al., 2024). A $\delta^{18}O_{sw}$ value (VSMOW) of −3.8 ‰ was measured in situ. Bivalve *Tridacna squamosa* (TS2) grew in a large zoo aquarium with an average water temperature of 25.9 °C and $\delta^{18}O_{sw}$ (VSMOW) of −1.05 ‰ (Batenburg et al., 2011).

2.2. Eocene samples

Eocene samples (Table 1) were collected from the Barton Clay Formation (base of the Naish Member) at Barton-on-Sea (southern UK). Five specimens were analysed: the gastropods *Sycostoma* sp. COX 1931 (sample FG1), *Orthosurcula rostrata* (SOLANDER 1766) (FG2), *Strombus athleta* (SOLANDER 1766) (FG3), and bivalves *Bathytormus sulcata* (SOLANDER 1766) (FM1) and *Arcturellina pusilla* (DESHAYES 1858) (FM2). The samples were collected from the same area as sample SW1 examined by Evans et al. (2018) from the Hampshire Basin, but are of a slightly younger age (39.5–40.5 Ma).

All Eocene mollusc shells consist of >99 % aragonite as determined by Powder X-Ray diffraction (XRD).

2.3. Sample preparation

In the case of samples RM1, RM2, RG1, and RG2 the entire shell was crushed to sub-cm sized fragments and then ground to a powder using an agate mortar and pestle. For samples WS2 and WS3 material was taken from the inner shell layer avoiding the muscle scars, ventral margin and palial sinus, umbo and hinge. These shells were first cleaned by abrading the outer layer with a rotary drill bit operated at its lowest speed and pressure.

Samples CHA_M_050 and CHA_M_062 consist of bulk powder

Table 2
Independently constrained growth temperatures, Δ_{47}-derived growth temperatures and independently constrained $\delta^{18}O_{SW}$ of investigated mollusc specimens.

Sample	Growth temperature	Δ_{47} derived T (°C)	T-range 95 % CI (°C)	$\delta^{18}O_{SW}$ (‰ vs VSMOW)
RG1	MASST 9.6 °C, Seasonal range 7–12.4 °C	6.9	4.7–9.0	0.2 (Harwood et al., 2008)
RG2	MASST 9.6 °C Seasonal range 7–12.4 °C	9.1	7.5–10.7	0.2 (Harwood et al., 2008)
RM1	MASST 9.6 °C Seasonal range 7–12.4 °C	8.2	6.0–10.5	0.2 (Harwood et al., 2008)
RM2	MASST 9.6 °C Seasonal range 7–12.4 °C	8.2	5.9–10.5	0.2 (Harwood et al., 2008)
AL_006	Cultured at 12 °C	12.3	10.0–14.6	−1.55
CHA_M_050	MASST 3.9 °C Seasonal range 1.8–7.4 °C	7.6	5.4–9.9	Approximate estimate ~ 0 (Schmidt et al., 1999)
CHA_M_062	MASST 3.9 °C Seasonal range 1.8–7.4 °C	5.1	2.9–7.4	Approximate estimate ~ 0 (Schmidt et al., 1999)
M2-Sf	MASST 11.5 °C Seasonal range 4.5–19.2 °C	19.0	16.9–21.1	−1.55
M2-Sv	MASST 11.5 °C Seasonal range 4.5–19.2 °C	12.1	10.2–14.0	−1.55
ME_002	Mean growth temperature 16.2 °C Seasonal range 5–25 °C	16.1	13.9–18.3	−1.55
ME_003	Mean growth temperature 16.2 °C Seasonal range 5–25 °C	15.4	13.1–17.7	−1.55
Shell UC	est. 27–31 °C (based on geographic occurrence)	26.3	24.0–28.7	~0.1 (Schmidt et al., 1999)
Shell UH	est. 27–31 °C (based on geographic occurrence)	28.3	26.1–30.5	~0.1 (Schmidt et al., 1999)
TS2	25.9 °C, up to 26.8 °C in summer	24.4	22.2–26.6	−1.05 (measured)
WS2	MASST 7.1 °C Seasonal range 0.3–13.0 °C	1.4	−0.4–3.2	−3.24
WS3	MASST 7.1 °C Seasonal range 0.3–13.0 °C	8.3	6.4–10.3	−3.24

homogenised from *A. islandica* collected from NE Iceland in 2010 (Staudigel et al., 2023a; Pederson et al., 2019). Bulk powder was removed as circular cores from periodic growth bands using a drill, and were subsequently homogenised with a mortar and pestle. Shell UH was analysed for fluid inclusion $\delta^{18}O$ prior to being homogenised, as described in Nooitgedacht et al. (2021).

In the case of TS2, a section was cut out of the inner shell layer and ground to a fine powder using an agate mortar and pestle.

The sample preparation for M2-Sf and M2-Sv is described in de Winter et al. (2021a). M2-Sf samples a sufficiently large portion of the shell to represent the mean annual temperature at which the specimen grew. M2-Sv is a sample that averages shell material formed throughout the second growth year of the specimen, although we note that growth rate might not be constant throughout the year.

In the case of ME_002, ME_003, and AL_006 the bulk shell parts that were grown in culture were sampled without differentiated sampling of the outer and inner shell.

The Eocene samples FG1, FG2, FG3, FM1, and FM2 were crushed to smaller pieces using a hammer. These pieces were cleaned by scraping clay residues off with a spatula and rinsing the shell fragments with deionised (DI) water in an ultrasonic bath. They were ground to powder with an agate mortar and pestle.

With the exception of samples RM1, RM2, RG1, and RG2, which were subjected to oxidative cleaning using a 3 wt-% NaOCl solution (Fiebig et al., 2024), the powders did not undergo any pre-treatment for organic matter removal. After reacting overnight, the NaOCl solution was discarded and the powders rinsed with DI water before being left to dry at room temperature for several days. All sample powders were stored in a vacuum dryer at 30 °C before isotopic analysis. Non-bleached aliquots (n = 6) of RG2 were analysed along with bleached (n = 9) aliquots. We did not detect any significant differences in the dual clumped isotope compositions for the two sets of sub-samples (see Supplementary Fig. S1). Thus, we conclude that interfering components that release NO_2 (Fiebig et al., 2024) were absent, and that oxidative cleaning did not affect the dual clumped isotope compositions of our sample powders. As such, both sub-sets of RG2 aliquots were pooled for the purpose of data interpretation.

2.4. Mass spectrometric analyses and data processing

All samples were analysed for their Δ_{47}, Δ_{48}, $\delta^{18}O$ and $\delta^{13}C$ values following the experimental setup of Fiebig et al. (2019) and methodology described by Bernecker et al. (2023). For dual clumped isotope measurements, 10 mg (±0.2 mg) per replicate were weighed into silver capsules; 6–15 replicates were analysed for each sample. Acid digestion took place in a common acid bath at 90 °C using phosphoric acid (>108 wt-%). ETH-1, ETH-2, non-bleached ETH-3, in-house Carrara marble as well as CO_2 gases equilibrated at 25 °C and 1000 °C, respectively, were analysed alongside the samples. The preparation process of equilibrated and heated gases followed the procedure described in Bernecker et al. (2023). All samples, standards, and gases were measured against a reference gas with the following isotopic compositions: $\delta^{13}C_{VPDB} = -4.2$ ‰ and $\delta^{18}O_{VSMOW} = 25.26$ ‰ (ISO-TOP, Air Liquide, France).

Dual clumped data processing followed the method described in Bernecker et al. (2023), using optimal scaling factors for pressure baseline correction based on continuously monitored *m/z* 47.5 intensities and slope minimisation algorithm for δ^{47} vs. Δ_{47} and δ^{48} vs. Δ_{48} correlations of equilibrated gas data. Background corrected raw data was normalised to the Carbon Dioxide Equilibrium Scale for an acid digestion temperature of 90 °C (CDES 90) (Dennis et al., 2011) using D47crunch (Daëron, 2021), pooling over all sessions and considering equilibrated gases as anchors exclusively. For this purpose, non-bleached replicates of ETH-3 were labelled individually in order to avoid any bias introduced by the variance algorithm of D47crunch (Fiebig et al., 2024). Reported uncertainties represent fully propagated 2 SE, considering allogenic and autogenic errors.

$\delta^{18}O$ values of carbonate samples analysed in this study were normalised against nominal values of ETH-1 and ETH-2 (Bernasconi et al., 2018). Since these ETH standards are calcite, the difference in acid fractionation factors between aragonite (ar) and calcite (cc) at 90 °C (Kim et al., 2007a) needs to be considered for the determination of aragonite $\delta^{18}O$. For this purpose, we considered Eq. (1):

$$\alpha_{CO_2-CaCO_3} = \frac{\delta^{18}O_{CO2} + 1000}{\delta^{18}O_{CaCO3} + 1000} \quad (1)$$

For aragonitic samples, in a first step, $\delta^{18}O$-CO_2 was determined based on the $\delta^{18}O_{CaCO_3}$ normalised to ETH-1 and ETH-2, applying the acid fractionation factor ($\alpha_{CO_2-CaCO_3}$) for calcite of 1.00813. In a second step, $\delta^{18}O$-CO_2 was inserted into Eq. (1) to determine the aragonitic $\delta^{18}O_{CaCO_3}$ using the aragonite-specific acid fractionation factor of 1.00854. For

samples of mixed mineralogy (*P. vulgata, M. edulis*), we considered an effective acid fractionation factor α_{eff} that was weighted to the percentile abundances of calcite (x_{cc}) and aragonite (1-x_{cc}) in the sample to calculate $\delta^{18}O_{CaCO_3}$:

$$\alpha_{eff} = x_{cc}\alpha_{CO_2-cc} + (1 - x_{cc})\alpha_{CO_2-ar} \quad (2)$$

2.5. Dual clumped isotope equilibrium

In order to identify kinetic bias in the dual clumped isotope compositions of molluscs and to determine apparent growth temperatures we compare measured Δ_{47}-Δ_{48} values with the Δ_{47}-Δ_{48}-T relationships of Fiebig et al. (2024). The latter has been reprocessed from original highest precision data published by Fiebig et al. (2021) to exclude any bias from isobaric contamination of ETH-3 (Fiebig et al., 2024). Over the temperature range of 8–1100 °C, the reprocessed Δ_{47}-Δ_{48}-T relationships depart by less than −1 ppm (Δ_{47}) and −3 ppm (Δ_{48}) from the original relationships of Fiebig et al. (2021). The validity of the Δ_{47}-T and Δ_{48}-T relationships of Fiebig et al. (2021, 2024) have been independently confirmed by Anderson et al. (2021) and Swart et al. (2021), respectively. In the low temperature range, the Δ_{47}-Δ_{48}-T relationship of Fiebig et al. (2024) is anchored against Devils Hole and Laghetto Basso carbonates. These two natural calcites were precipitated at extremely slow growth rates (< 1 μm/yr; Daëron et al., 2019), which brings them closest to the equilibrium limit of precipitation (Watkins et al., 2013, 2014) at which dissolution and precipitation rate of calcite become approximately equal. We, therefore, consider the Δ_{47}-Δ_{48}-T relationships of Fiebig et al. (2024) to reflect the most accurate and precise estimation of the position of Δ_{47}/Δ_{48} equilibrium that is currently available.

2.6. Re-evaluating the temperature dependence of the oxygen isotope fractionation between mollusc carbonate and water

We compiled aragonite, calcite, and seawater $\delta^{18}O$ data from Grossman and Ku (1986), Lecuyer et al., (2004, 2012), Henkes et al. (2013), Caldarescu et al. (2021), Huyghe et al. (2022), and de Winter et al. (2022) to re-evaluate the temperature dependence of the oxygen isotope fractionation between mollusc shell-carbonate and seawater. We additionally included data from the modern specimens investigated here (Tables 1, 2), using directly measured temperatures for culture experiments and mean annual temperatures for naturally sampled specimens. The compiled data sets are available in Supplementary Table S1. De Winter et al. (2022) originally provided high-resolution data from four specimens, so we calculated specimen-specific mean $\delta^{18}O$ values from their data in order to avoid over-representation. The aragonitic samples of Grossmann and Ku (1986) were acid digested at 50–60 °C and calibrated against NBS 19 calcite. In order to account for the difference in acid fractionation factors between aragonite and calcite, we, therefore, considered the equation for acid fractionation for calcite by Kim et al. (2007a) (T = 55 °C; $\alpha_{CO_2-cc} = 1.00919$) to calculate $\delta^{18}O_{CO_2}$ from the given $\delta^{18}O_{CaCO_3}$ and then their equation for aragonite (T = 55 °C; $\alpha_{CO_2-ar} = 1.00955$) to obtain aragonitic $\delta^{18}O_{CaCO_3}$, as detailed in section 2.4. Oxygen isotope fractionation factors of aragonite and calcite with respect to water were calculated from published oxygen isotope compositions according to (3)

$$\alpha_{CaCO_3-H_2O} = \frac{\delta^{18}O_{CaCO3} + 1000}{\delta^{18}O_{H_2O} + 1000} \quad (3)$$

Uncertainties for oxygen isotope and temperature input data are not consistently reported in the studies of Grossman and Ku (1986), Lecuyer et al. (2004, 2012), Henkes et al. (2013), Caldarescu et al. (2021), Huyghe et al. (2022) and de Winter et al. (2022). An error-weighted linear regression would, therefore, add more weight to data that lacks any reported uncertainties, which needs to be avoided. Consequently, we did not consider uncertainties in compiled $\alpha_{CaCO_3-H_2O}$ values and growth temperatures in the computation of linear regressions.

3. Results

Bulk stable and clumped isotope compositions of all modern and fossil specimens analysed in this study are listed in Tables 3 and 4, respectively. Baseline-corrected input data (δ^{45}-δ^{49}) as well as Δ_{47}, Δ_{48}, $\delta^{18}O$, and $\delta^{13}C$ results, along with processing statistics, can be found in Supplementary Tables S2 and S3.

3.1. Clumped isotopes

Dual clumped isotope data of the molluscs is compared to the position of equilibrium (Fiebig et al., 2021, revised after Fiebig et al., 2024) in Fig. 1 for modern samples and in Fig. 2 for Eocene samples. With the exception of one specimen (RG2), all modern and Eocene molluscs plot indistinguishably from the Δ_{47}-Δ_{48} equilibrium line. Δ_{47}-derived temperatures obtained from modern and fossil specimen are listed in Table 2 and Table 4, respectively. A correlation plot of disequilibrium Δ_{47} vs. disequilibrium Δ_{48} of modern specimens is provided in Supplementary Fig. S2. Here, disequilibrium Δ_i corresponds to the difference between measured Δ_i and Δ_i predicted by habitat temperature based on the Δ_{47}-Δ_{48}-T relationship of Fiebig et al. (2024). Taking analytical and seasonal temperature variations into account, RG2 is the only sample that plots outside of uncertainty from equilibrium, i.e., from the expected range of equilibrium Δ_{47}-Δ_{48} values (Supplementary Fig. S2).

Visual inspection of Fig. 1 implies that samples in the lower temperature range, may, on average, plot further from the equilibrium line than their higher temperature counterparts. In order to quantitatively test if the dual clumped isotope composition of carbonate from organisms characterised by relatively low mean annual growth temperatures (T < 10 °C, group (1); n = 8) is characterised by a greater degree of scatter around the equilibrium line than those grown at higher temperatures (T > 10 °C, group (2); n = 8) we determined the absolute distance of each data point from the equilibrium line. Namely, the absolute difference between measured Δ_{48} and the Δ_{48} value displayed for the same sample by horizontal projection of its measured Δ_{47} value to the equilibrium line. We performed a *t*-test to investigate whether the mean absolute distance displayed by group (1) data is different to that derived from group (2). The *t*-test reveals mean absolute distances of 16.1 ± 1.6 ppm (1 SE) and 4.6 ± 1.3 ppm for group (1) and group (2), respectively. A p-value of 0.0003 indicates the two populations are distinguishable from each other, highlighting that organisms with growth temperatures < 10 °C exhibit significantly larger departures from the Δ_{47}-Δ_{48} equilibrium line than those living in warmer water masses (T > 10 °C).

3.2. Oxygen isotope fractionation between water and carbonate

1000lnα($CaCO_3$-H_2O)-1/T relationships for aragonite and calcite are displayed in Figs. 3a and b, respectively, yielding the following Eqs. (4) and (5):

$$1000ln(\alpha_{ar-H_2O}) = 16.483\,(\pm 0.424) \times (10^3/T) - 25.77\,(\pm 1.46), \quad R^2 = 0.90,\ n = 154 \quad (4)$$

$$1000ln(\alpha_{cc-H_2O}) = 15.663\,(\pm 0.832) \times (10^3/T) - 23.62\,(\pm 2.87), \quad R^2 = 0.81,\ n = 81 \quad (5)$$

In order to constrain the sensitivity of the regressions to possible outliers in the two data sets, we compare the above ordinary least-squares regression to those resulting from a bootstrapping approach, in which the individual data sets were randomly resampled 10,000 times, adding

Table 3
Stable and clumped isotope data of the investigated molluscs. n represents the number of mollusc specimens analysed.

Sample	$\delta^{18}O_{CO_2}$ VSMOW [‰]	$\delta^{18}O_{CC}$ VSMOW [‰]	$\delta^{18}O_{CC}$ VPDB [‰]	$\delta^{13}C$ VPDB [‰]	Δ_{47} CDES90 [‰]	Δ_{47} 95 % CI [‰]	Δ_{48} CDES90 [‰]	Δ_{48} 95 % CI [‰]	n
Modern									
RG1	41.31	32.50	1.53	1.12	0.6493	0.0068	0.2550	0.0210	9
RG2	40.99	32.60	1.63	0.93	0.6422	0.0050	0.2882	0.0159	21
RG2*	40.93	32.48	1.51	0.90	0.6441	0.0056	0.2904	0.0180	15
RG2_U	41.13	32.68	1.71	1.01	0.6377	0.0078	0.2836	0.0244	6
RM1	41.12	32.30	1.34	1.49	0.6450	0.0071	0.2545	0.0214	9
RM2	41.03	32.21	1.25	0.77	0.6451	0.0074	0.2500	0.0223	8
AL_006	41.79	32.97	1.99	0.05	0.6324	0.0070	0.2713	0.0225	7
CHA_M_050	42.76	33.96	2.95	1.29	0.6468	0.0071	0.2620	0.0231	7
CHA_M_062	43.19	34.36	3.34	2.30	0.6548	0.0072	0.2639	0.0232	7
M2-Sf	37.58	29.21	−1.66	−2.00	0.6122	0.0065	0.2644	0.0215	8
M2-Sv	37.72	29.35	−1.52	−1.84	0.6336	0.0062	0.2654	0.0204	9
ME_002	39.26	30.88	−0.04	−1.70	0.6209	0.0066	0.2535	0.0209	8
ME_003	39.19	30.81	−0.11	−1.41	0.6229	0.0070	0.2600	0.0221	7
Shell UC	37.99	29.20	−1.67	2.91	0.5909	0.0066	0.2425	0.0204	8
Shell UH	37.72	28.93	−1.93	2.44	0.5855	0.0062	0.2384	0.0194	9
TS2	36.69	27.91	−2.92	−7.42	0.5965	0.0064	0.2400	0.0214	8
WS2	41.21	32.39	1.43	1.64	0.6668	0.0059	0.2595	0.0187	10
WS3	37.30	28.52	−2.33	−0.05	0.6446	0.0061	0.2864	0.0195	9
Fossil									
FG1	36.61	27.83	−3.00	0.08	0.6171	0.0068	0.2420	0.0206	9
FG2	36.96	28.18	−2.66	−2.08	0.6076	0.0066	0.2563	0.0206	9
FG3	36.65	27.87	−2.96	−1.88	0.6082	0.0067	0.2391	0.0205	9
FM1	37.14	28.36	−2.48	1.20	0.6071	0.0068	0.2488	0.0209	9
FM2	35.73	26.96	−3.84	0.58	0.5999	0.0067	0.2433	0.0207	9

Table 4
Δ_{47}-derived temperatures and reconstructed seawater $\delta^{18}O$ for the Eocene samples.

Sample	Δ_{47} derived T (°C)	T-range 95 % CI (°C)	Reconstructed $\delta^{18}O_{sw}$ (‰ vs VSMOW)	$\delta^{18}O_{SW}$-range 95 % CI (‰ vs VSMOW)
FG1	17.3	15.1–19.6	−3.4	−2.9 – −3.8
FG2	20.5	18.3–22.8	−2.4	−2.0 – −2.8
FG3	20.3	18.1–22.6	−2.7	−2.3 – −3.2
FM1	20.7	18.4–23.1	−2.2	−1.7 – −2.6
FM2	23.2	21.0–25.6	−3.1	−2.6 – −3.5

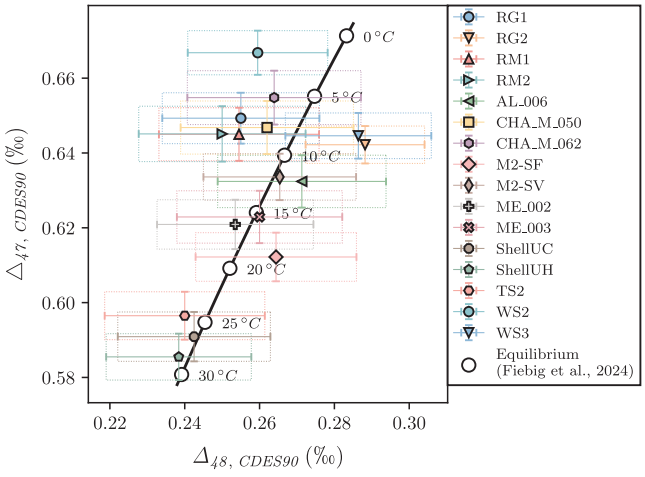

Fig. 1. Dual clumped isotope composition of modern molluscs. Δ_{47}/Δ_{48} values are shown relative to the position of equilibrium (Fiebig et al., 2024). Error bars represent fully propagated 2SE.

higher weight to random individual samples by resampling with replacement. Each outcome was fit using ordinary least-squares regression again. The overall results, based on the 50th percentile of

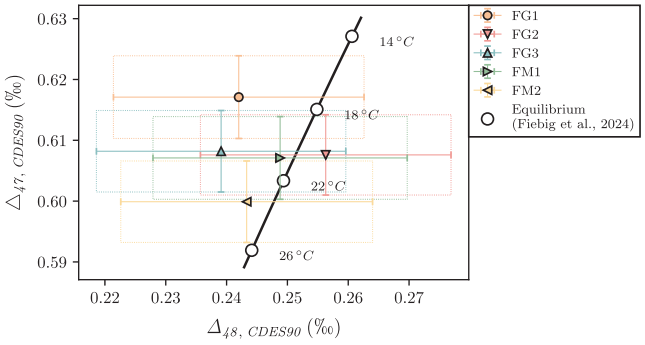

Fig. 2. Dual clumped isotope composition of the Eocene mollusc samples. Δ_{47}/Δ_{48} values are shown relative to the position of equilibrium (Fiebig et al., 2024). Error bars represent fully propagated 2SE.

the 10^4 regression coefficients, are shown in Supplementary Fig. S3. These demonstrate that the difference between the original and resampled approach results in calibrations that differ by less than 0.12 ‰ across the entire investigated temperature range.

4. Discussion

4.1. Dual clumped isotope thermometry on modern mollusc shells

Although most modern samples have dual clumped isotope compositions that fall within uncertainty of equilibrium, this observation, on its own, does not provide unambiguous evidence that equilibrium has been attained in each case. A comparison of measured growth temperatures with Δ_{47}-derived growth temperatures is necessary to prove this hypothesis in more detail. This comparison allows us to identify samples that have been affected by two or more rate-limiting kinetic processes which – in combination – could lead to Δ_{47} and Δ_{48} values plotting fortuitously indistinguishable from equilibrium, as was observed for individual brachiopods (Davies et al., 2023).

Δ_{47}-derived temperatures for samples *B. undatum* (RG1), *M. modiolus*

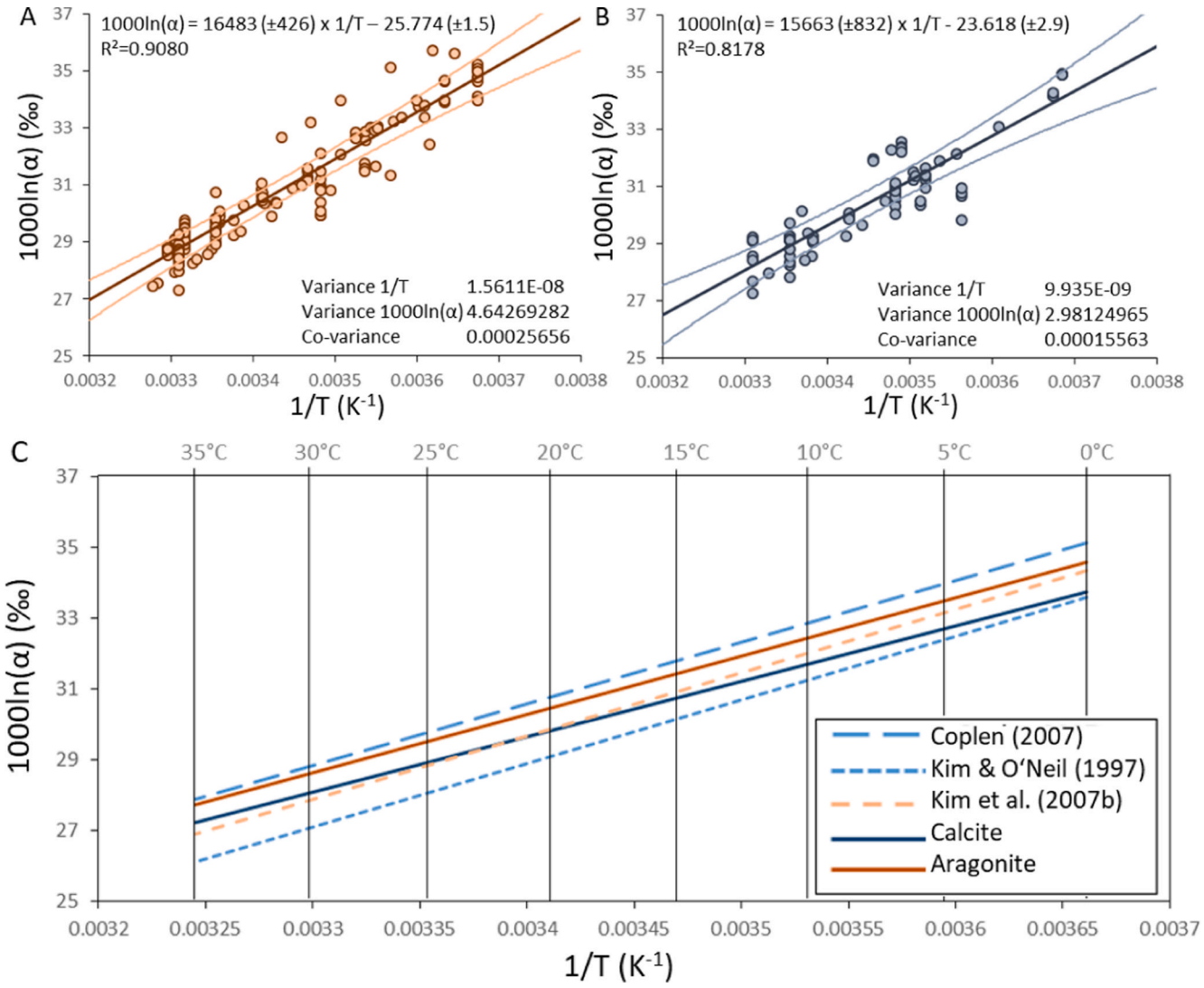

Fig. 3. Temperature dependence of the oxygen isotope fractionation between water and calcite and aragonite, respectively. Compilation of empirical oxygen isotope fractionation data for aragonitic (A; in orange; n = 154) and calcitic (B; in blue; n = 81) molluscs (Grossman and Ku, 1986; Lécuyer et al., 2004, 2012; Henkes et al., 2013; Caldarescu et al., 2021; de Winter et al., 2022; Huyghe et al., 2022; this study). Growth temperatures reflect measured water temperatures. For linear regressions (thick lines) in A and B, uncertainties in growth temperatures and 1000lnα were not considered as these were not consistently reported in each of these studies. Thin lines in A and B represent 95 % confidence intervals of regression lines. A comparison of corresponding empirical regression lines with inorganic relationships obtained by Coplen (2007) and Kim & O'Neil (1997) for calcite, and Kim et al. (2007b) for aragonite is shown in C.

(RM1) and *S. solida* (RM2), which are apparently in equilibrium (Fig. 1), are 6.8 °C (±2.2 °C, 95CI), 8.2 °C (±2.3 °C) and 8.2 °C (±2.4 °C), respectively. These values agree with the mean annual sea surface temperature (MASST) of 9.6 °C and/or the seasonally monitored temperature range of 7.0–12.4 °C reported for the beach at Tentsmuir Forest within their errors (Table 2, Supplementary Fig. S2). A fourth sample, *P. vulgata* (RG2) was collected at the same sample location. Its Δ_{47}-derived temperature of 9.1 °C (±1.6 °C) is consistent with the MASST of 9.7 °C (Table 2); however, its Δ_{48}-value exhibits a slightly positive, but significant bias relative to the equilibrium Δ_{48}-value expected for this temperature (Fig. 1; Supplementary Fig. S2). Fiebig et al. (2024) found that NO_2 interferent can cause $-\Delta_{47}/+\Delta_{48}$ offsets from equilibrium, but NO_2 bias can be excluded in this case since the mean Δ_{47} and Δ_{48} values of bleached and unbleached aliquots of that sample were indistinguishable from each other (Supplementary Fig. S1). The outer and inner shell areas of gastropod RG2 consist of calcite and aragonite, respectively; such that our powder sample is of mixed mineralogy. The $\delta^{18}O$ values of both phases, however, differ by less than 1 ‰ such that non-linear mixing also cannot explain the observed offset from equilibrium (Staudigel et al., 2023a, b; White & Defliese, 2023). Since artificial biases like mixing and NO_2 interference can be excluded, the observed disequilibrium signature of RG2 may, therefore, be of a kinetic nature that needs to be explored in more detail.

Δ_{47}-derived temperatures for all three specimens of *A. islandica* (AL_006, CHA_M_050, and CHA_M_062), all of which plot indistinguishably from equilibrium (Fig. 1), align with the independently known growth temperature ranges (Table 2; Supplementary Fig. S2). In the case of AL_006, which was grown in culture at a constant temperature of 12.0 °C, we reconstruct a temperature of 12.3 °C (±2.3 °C). CHA_M_050 and CHA_M_062 were collected from the NE Iceland margin alongside molluscs analysed in Pederson et al. (2019). The Δ_{47}-derived temperatures for these samples are 7.6 °C (±2.3 °C) and 5.1 °C (±2.3 °C), respectively. A mean annual water temperature of 3.9 °C was estimated for the site of sample collection, although the temperature can reach 7.4 °C during summer (Table 2). We therefore conclude the most likely explanation for this offset towards warmer temperature reconstructions may be due to preferential shell growth during summer months as has been observed for some molluscs (e.g., Vitahkari et al.,

2016; Witbaard et al., 1994; Goodwin et al., 2001; Kaandorp et al., 2003; Judd et al., 2017; de Winter et al., 2021a, b).

The sampled parts of the mussels *M. edulis* ME_002 and ME_003 were cultured at 5–25 °C with a mean temperature of 16.2 °C, although temperature was briefly raised/lowered to 31 °C and 3 °C, respectively, over a short period of time for the purpose of conducting respiration rate experiments (Jansen et al., 2007). Δ_{47}-derived temperatures for ME_002 and ME_003 are 16.1 °C (±2.2 °C) and 15.4 °C (±2.3 °C), respectively (Table 2), aligning well with estimated mean growth temperatures and, therefore, confirming that dual clumped isotope equilibrium has been attained (Fig. 1; Supplementary Fig. S2).

Samples of the oyster *M. gigas* (M2-Sf and M2-Sv) also plot indistinguishably from the equilibrium line within uncertainty (Fig. 1; Supplementary Fig. S2). These samples were taken from the same oyster shell. Measured Δ_{47}-values correspond to temperatures of 19.0 °C (±2.2 °C) and 11.9 °C (±2.0 °C), respectively (Table 2). The sample powders originate from two different small areas of the shell with different microstructures, i.e., from the foliated calcite in the hinge (M2-Sf) and from the chalky calcite material of the second growth year (M2-Sv) (see de Winter et al., 2021a, b for more information). Both sample powders represent averages of material grown across seasons, with their Δ_{47}-derived temperatures therefore potentially representing either mean annual or seasonal temperature, depending on when growth occurred (seasonal range of growth temperatures: 4.5–19.2 °C, mean: 11.5 °C, Table 2). M2-Sf exhibits a Δ_{47} temperature that corresponds to the maximum seasonal temperature. The colder Δ_{47}-derived formation temperature of 11.9 °C (±2.0 °C) for M2-Sv, on the contrary, is in excellent agreement with the measured mean annual temperature of 11.5 °C. The different temperatures obtained for M2-Sf and M2-Sv might stem from sampling bias. Given that the two samples are from the same shell a different calcification response to temperature change would not be expected. Instead, considering that only small areas were sampled, it is more likely that the powders represent different seasonal stages of growth.

Three *Tridacninae* from both the natural environment and an aquarium, including two different species, were analysed. The samples from a specimen of *H. porcellanus* (Shell UC and Shell UH) plot indistinguishably from the equilibrium line (Fig. 1) and yield Δ_{47}-derived growth temperatures of 26.4 °C (±2.3 °C) and 28.3 °C (±2.2 °C), respectively (Table 2). These temperatures match independently constrained habitat temperatures of 27–31 °C. *T. squamosa* (TS2), which also plots indistinguishably from the equilibrium line within uncertainty (Fig. 1), was cultured in an aquarium kept at near-constant temperature. The Δ_{47}-derived temperature of 24.4 °C (±2.2 °C) agrees with the mean growth temperature of 25.9 °C (up to 26.8 °C during summer) (Batenburg et al., 2011; Janse et al., 2008) within uncertainty (Table 2).

H. arctica (WS2) and *T. borealis* (WS3) from the White Sea plot above the equilibrium line, but in both cases their corresponding 2 SE boxes still overlap with the equilibrium line (Fig. 1). The Δ_{47}-derived temperature of 8.3 °C (±2.0 °C) for WS3 agrees within uncertainty with the estimated MASST of 7.1 °C (Table 2). WS2 still intersects the equilibrium line at its lower boundary level of Δ_{47} uncertainty. This intersection reflects a temperature of 3.2 °C which is lower than MASST, but is still within the range of seasonal surface temperatures characteristic of the White Sea (0.3–13 °C; Table 2). Supplementary Fig. S2 confirms that WS2 plots indistinguishably from equilibrium if the seasonal temperature range is considered.

Overall, most specimens that have dual clumped isotope compositions indistinguishable from equilibrium are characterised by Δ_{47}-derived temperatures that are in good agreement with observed (seasonal) growth temperatures. This strongly implies that the internal arrangement of heavy isotopes during $CaCO_3$ precipitation often proceeds up to equilibrium. Bulk mollusc shell samples may, therefore, provide a robust archive for accurate and highly precise temperature reconstructions by means of Δ_{47} thermometry. Potential seasonal biases due to preferential growth during summer need to be considered, especially when analysing bulk shells from mid-high latitude regions. At relatively low growth temperatures < 10 °C, kinetic limitations may become increasingly relevant. In this temperature range, mean Δ_{48} values depart significantly farther from the equilibrium line than at T > 10 °C (see section 3.1), and one out of eight specimen exhibits disequilibrium dual clumped isotope signatures. A more detailed investigation on multiple specimens per species are necessary to confirm whether disequilibrium Δ_{47} and Δ_{48} signatures in molluscs occur more often in the low temperature range. Until proven otherwise, care should be taken if Δ_{47} indicates temperatures < 10 °C, and, if possible, Δ_{48} be analysed along with Δ_{47} in order to identify potential kinetic bias.

4.2. Key parameters affecting biomineralisation of molluscs

Our observation that most of the investigated bivalve molluscs form their shells close to equilibrium differs from what is known about several other marine calcifying organisms. For example, corals have been shown to exhibit disequilibrium dual clumped isotope compositions, which has been proposed to be the result of CO_2 absorption during biomineralisation (Bajnai et al., 2020; Davies et al., 2022). Corals actively elevate the pH at their site of calcification (SOC) above that of ambient seawater, due to addition of Ca^{2+} or Na^{+} into the calcifying fluid and charge-balance-removal of H^{+} (e.g.; Spooner et al., 2016; Venn et al., 2019). During this process, aqueous CO_2 from ambient seawater and/or the ambient tissue cells diffuses into the SOC along its concentration gradient. At the SOC, this CO_2 is then transformed into bicarbonate via hydration/hydroxylation. These two reactions and their reverse reactions, dehydration/dehydroxylation, can be rate-limiting in the DIC-water-$CaCO_3$ system, and, therefore, in the accompanying oxygen isotope exchange among the different DIC species and water (McConnaughey, 1989b; Adkins et al., 2003; Sade and Halevy, 2017; Affek, 2013; Guo, 2020). Protonation/deprotonation of carbonate/bicarbonate, on the contrary, occurs almost instantaneously such that metastable chemical and isotopic equilibrium between both species is obtained at any time (McConnaughey, 1989b; Adkins et al., 2003; Chen et al. 2018). Achieving oxygen and clumped isotope equilibrium in the DIC-H_2O system thus depends on the relative rates of CO_2 hydration/hydroxylation, bicarbonate dehydration/dehydroxylation and precipitation. If precipitation proceeds faster than isotopic equilibration of the DIC pool, disequilibrium signatures will be recorded in the forming carbonate (e.g., McConnaughey, 1989b; Adkins et al., 2003; Chen et al. 2018; Guo & Zhou, 2019; Guo, 2020; Bajnai et al., 2020). In the case of cold and warm water corals, the dehydration/dehydroxylation reactions are slowest such that the isotopic composition of the precipitated carbonate largely records the kinetic isotope effects associated with the hydration/hydroxylation reactions of CO_2, resulting in lighter-than-equilibrium $\delta^{18}O$, $\delta^{13}C$, and Δ_{48}, but heavier Δ_{47} (Davies et al., 2022).

In the case of molluscs, the extrapallial fluid (EPF), in which precipitation takes place, is enclosed by the calcifying cells of the mantle epithelium as well as the periostracum, an organic layer covering the shell and extending over its edge (Fig. 4). The intra-cellular pH of the mantle cells is known to be around 7.4–7.5, while the EPF is characterised by a pH of ~ 7.8 (Ip et al., 2006) but may be as low as 7.2 (Crenshaw, 1972). The cytosol of the surrounding cells is slightly more acidic than the EPF, which results in diffusion of (metabolic) CO_2 from the surrounding cells into the EPF. The rate of (de)hydration/(de)hydroxylation reactions, and thus the rate at which isotopic equilibration of the DIC-H_2O system is achieved, is largely affected by factors such as pH and temperature, with higher pH and lower temperatures resulting in slower isotopic equilibration rates (e.g., Guo, 2020). The rate-dependence of the attainment of equilibrium on pH might offer an explanation for why molluscan shell carbonates exhibit equilibrium dual clumped isotope compositions while skeletons of corals do not. Unlike corals, which elevate the pH at the SOC above seawater pH to initiate calcification, the pH of the EPF is lower than that of seawater (which in molluscs is the equivalent to the SOC in corals) by 0.5–0.6 units (cf.

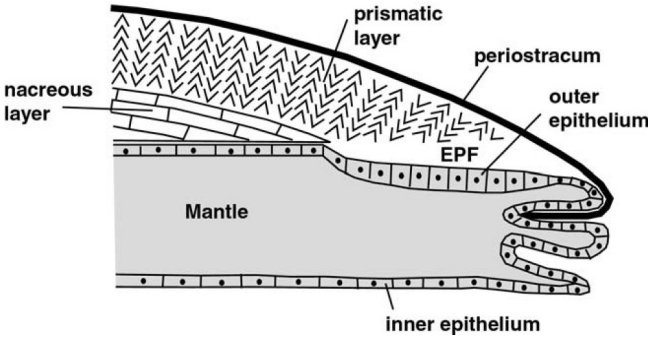

Fig. 4. Schematic drawing of the EPF (taken from Carré et al., 2006). Shell formation in molluscs is orchestrated within the extrapallial fluid (EPF) which is enclosed by the outer epithelium (outermost cell layer of the mantle) and the periostracum (organic layer that covers the shell).

Crenshaw, 1972). At 25 °C, isotopic equilibration of the DIC-H_2O system at a pH of 7.7 is predicted to proceed five times faster than at a pH of 8.7 that likely prevails at the SOC of some corals (e.g., Ross et al., 2022 and references therein) (Guo, 2020). At 10 °C and 5 °C, on the contrary, the overall equilibration rate at a pH of 7.7 is reduced by a factor of 3 and 5, respectively, relative to 25 °C. The absolute rate of equilibration furthermore depends on the absence/presence of the enzyme carbonic anhydrase (CA). CA catalyses the hydration of CO_2 (e.g., Freeman and Wilbur, 1948; Nielsen and Frieden, 1972; Uchikawa and Zeebe, 2012; Le Roy et al., 2016) using Zn^{2+} as central ion in order to polarise, and therefore activate, water for the reaction (Park & Lee, 2019). The presence of CA has been observed in both corals (e.g., Uchikawa and Zeebe, 2012; Bertucci et al., 2013) and molluscs (e.g., Freeman and Wilbur, 1948; Nielsen and Frieden, 1972). CA has been found to be directly involved in molluscan shell formation, e.g., in the matrix during nacre production (Marie et al., 2008), as domain in nacrein (a protein important for nacre-formation) (Miyamoto et al., 1996) as well as in the mantle cells (Cardoso et al., 2019). In molluscs, proteins like nacrein inhibit calcium carbonate crystallisation from supersaturated solutions (Miyamoto et al., 2005), possibly to enable the organisms to tightly control the rate of calcification. In addition to pH and temperature, the presence of CA and nacrein may, therefore, act to result in the attainment of equilibrium in the molluscan DIC-H_2O-$CaCO_3$-system.

4.3. Kinetic biases and the potential impact of sample habitat

The increased scatter around the Δ_{47}-Δ_{48} equilibrium line at temperatures < 10 °C may indicate that (de)hydration/(de)hydroxylation reactions slowly become rate-limiting at low temperatures. CO_2-absorption is known to introduce $+\Delta_{47}/-\Delta_{48}$ offsets from dual clumped isotope equilibrium and has been shown to be of importance in other biogenic carbonates such as corals and brachiopods (Davies et al., 2022, 2023). CO_2 degassing, on the contrary, goes along with $-\Delta_{47}/+\Delta_{48}$ offsets from equilibrium and has been postulated to be effective in bivalve molluscs (Curley et al., 2023).

A single measured sample of *P. vulgata* (RG2) plots below the equilibrium line in dual clumped isotope space (Fig. 1). Its Δ_{47} value, however, corresponds to MASST at its growth site (Table 2). *P. vulgata*, a common limpet occupying an intertidal habitat, is submerged at high tides and exposed to air at low tides. Gas exchange with the surrounding environment during times of emersion is restricted in order to prevent desiccation (e.g., Burnett, 1988). To counteract the resulting hypercapnia (i.e., the accumulation of metabolic CO_2 which leads to acidification of the haemolymph) parts of the (inner) shell are dissolved (Lindinger et al., 1984). During this process, the DIC concentration of the EPF thus increases. It has been postulated that CO_2-degassing might occur as soon as the mollusc is submerged again and gas exchange with the surrounding water resumes (Curley et al., 2023). It has also been postulated that calcification rates in intertidally living species are accelerated during times of submersion (Tagliarolo et al., 2013a, b) but cease during emersion. This acceleration of growth rate may be explicable by the fact that the organism is in contact with seawater, from which the ions for calcification are ultimately derived, for less time than subtidal species, of relevance because an accelerated growth rate in combination with CO_2 degassing may result in disequilibrium bias. In addition, amorphous calcium carbonate (ACC) has been observed in some species (Weiss et al., 2002; Nassif et al., 2005; Jacob et al., 2011), representing a transient precursor of more stable crystalline aragonite or calcite (see e.g., Addadi et al., 2003, 2006). Tagliavento et al. (2023) showed that high Mg-calcite formed via amorphous calcium magnesium carbonate (ACMC), exhibited a significant $+\Delta_{48}$ bias relative to the Δ_{48} calcite equilibrium value predicted by its formation temperature, whereas its Δ_{47} corresponded to that temperature. The positive disequilibrium Δ_{48} bias of RG2 may, therefore, imply that ACC is involved in the biomineralisation process of *P. vulgata*. If so, the absence of such a bias in *M. edulis* (samples ME_002 and ME_003), in which aragonite and calcite production has been shown to proceed via ACC (Fitzer et al., 2016), would indicate that the $+\Delta_{48}$ bias of ACC can be subsequently overprinted during its transformation to the final polymorph.

Based on the analysis of a single specimen we cannot identify which process is responsible for the apparent disequilibrium signal in RG2. It should also be borne in mind that one of the ~20 samples reported here is statistically expected to fall outside of uncertainty of the dual clumped isotope equilibrium line based on its fully propagated 95 % confidence interval. More dual clumped isotope data on intertidal species is required to investigate if their isotopic compositions are affected by kinetic isotope effects. While *M. gigas* as well as *M. edulis* also occur in intertidal habitats and therefore could help resolve this issue, there were no tidal cycles present during the time period of culture experiments in which these specimens were grown. Future studies using dual clumped isotopes should also confirm whether kinetic limitations occur in the inner shell layer, as postulated previously (Curley et al., 2023).

4.4. Oxygen isotope fractionation into aragonitic and calcitic mollusc shells

It is still unknown if, and to what extent, the temperature dependence of equilibrium oxygen isotope fractionation between aragonite and water differs from that between calcite and water. Attempts to determine such equilibrium relationships have been made using inorganic precipitation under controlled conditions (e.g., Dietzel et al., 2009; Kim et al., 2007b; Kim and O'Neil, 1997; Wang et al., 2013; Watkins et al., 2013) and through theoretical calculations (e.g., Schauble et al., 2006; Hill et al., 2014), although these theoretical computations yielded inconsistent results. Whereas Hill et al. (2014) predicted a 1.3 ‰ fractionation in $\delta^{18}O$ values between aragonite and calcite at 25 °C, the results of Schauble et al. (2006) suggest no significant fractionation between these two minerals at the same temperature. Inorganic precipitation experiments revealed that the oxygen isotope fractionation between calcite and water can vary with pH (due to the kinetic isotope effects (KIEs) associated with CO_2-bicarbonate interconversion) and precipitation rate (e.g., Dietzel et al., 2009). While Kim & O'Neil (1997) proposed an equilibrium 1000lnα(calcite-H_2O)-1/T relationship, they achieved supersaturation and calcite precipitation via the continuous removal of CO_2 from Na-Ca-HCO_3^- solutions and did not report if oxygen isotope equilibrium between DIC species and water was attained prior to the onset of precipitation. In addition, that study precipitated $CaCO_3$ along a pH gradient in the absence of carbonic anhydrase at rates which are insufficient to maintain oxygen isotope equilibrium in the $CaCO_3$-DIC-H_2O system during progressive precipitation (Watkins et al., 2014).

It is now widely accepted that the indistinguishable 1000lnα($CaCO_3$-H_2O)-1/T relationships of Coplen (2007) and Däeron et al. (2019) are closest to equilibrium. These relationships were derived from natural

subaqueous calcites that precipitated at extremely low rates (< 1 μm/yr) at which the dissolution rate approaches the precipitation rate (Watkins et al., 2013, 2014). In the temperature range of 0–40 °C, the 1000lnα-1/T relationship of Coplen (2007) differs from the aragonite equilibrium relationship proposed by Kim et al. (2007b) by 0.8 to 1.0 ‰. It remains unlcear if oxygen isotope equilibrium has been attained in the aragonite precipitation experiments of Kim et al. (2007b). Aragonite is metastable at ambient temperatures, and calcite precipitation was kinetically inhibited via the addition of Mg^{2+}.

There is currently no indication from clumped isotope measurements that aragonite and calcite behave differently at equilibrium (e.g., Defliese et al., 2015; de Winter et al., 2022; Bernecker et al., 2025). Our results support these previous findings. With the exception of RG2, M2-Sf, M2-Sv, ME_002 and ME_003 all molluscs analysed in this study are entirely composed of aragonite. These aragonitic specimens exhibit dual clumped isotope compositions that are indistinguishable from the inorganic calcite equilibrium-Δ_{47}-Δ_{48}-T relationship (Fig. 1). Moreover, their Δ_{47} values correspond to independently constrained habitat temperatures (see section 4.1).

To investigate potential mineralogical differences in mollusc-specific 1000lnα($CaCO_3$-H_2O)-1/T relationships we compiled the available datasets for aragonite (Fig. 3a) and calcite (Fig. 3b). Linear regressions obtained on these two datasets are compared to the inorganic calcite-water relationships of Coplen (2007) and Kim & O'Neil (1997), and to the inorganic aragonite-water relationship of Kim et al. (2007b) in Fig. 3c. We find that calcitic molluscs exhibit oxygen isotope fractionations closer to the equilibrium fractionation of Coplen (2007) at warmer temperatures (Fig. 3c). On the contrary, at colder temperatures, the molluscan calcite fractionation line approaches the (kinetically biased) regression line published by Kim and O'Neil (1997).

Over the investigated range of 0–40 °C, at any given T, the oxygen isotope fractionation between aragonitic molluscs and seawater is 0.5 to 1.0 ‰ larger than that between calcitic molluscs and seawater (Fig. 3c). Aragonitic molluscs display the same behaviour as their calcitic counterparts; the corresponding oxygen isotope fractionations approach values predicted by Coplen (2007) at the upper end of the temperature range covered by the data (~30 °C), but increasingly deviate from the latter with decreasing temperature, approaching the experimental aragonite relationship published by Kim et al. (2007b) at 0 °C.

Our observation that the oxygen isotope fractionation between aragonite and water approaches values predicted by Coplen (2007) at elevated temperatures may indicate that aragonite and calcite share the same 1000lnα($CaCO_3$-H_2O)-1/T equilibrium relationship, but that the attainment of isotopic equilibrium with water is kinetically inhibited at common Earth-surface temperatures. The observed differences in the magnitude of oxygen isotope fractionation between aragonite and calcite might be due to small differences in KIEs prevalent at the mineral-fluid interface during mineral formation. These interfacial KIEs might differ in extent depending on the forming polymorph, for example, because detachment/attachment kinetics (Watkins et al., 2013; 2014) may depend on the characteristics of the mineral surface which, in turn, may depend on the respective polymorph that is forming. Alternatively, the high level of supersaturation required for aragonite precipitation may, for a given pH and temperature, proceed with faster interconversion between dissolved CO_2 and bicarbonate.

Above a temperature of 10 °C, at which kinetic departures from Δ_{47} and Δ_{48} equilibrium values may become inconsequential (Fig. 1), our empirical mollusc-specific 1000lnα($CaCO_3$-H_2O)-1/T relationships for aragonite and calcite depart from that of Coplen (2007) by up to −0.5 ‰ and −1.2 ‰, respectively (Fig. 3c). It was noticed in several studies that the Δ_{47} composition of carbonate precipitates did not correlate with the oxygen isotope fractionation between carbonate and water if this fractionation deviated from that predicted by Coplen (2007) by less than −1.5 ‰ (e.g., Kelson et al., 2017; Levitt et al., 2018; Jautzy et al., 2020; Fiebig et al., 2021). The observed discrepant behaviour between clumped and oxygen isotopes may support the hypothesis that interfacial isotopic equilibration occurs faster for clumped than for oxygen isotopes (Tripati et al., 2015; Levitt et al., 2018), such that there exists a precipitation regime where DIC disequilibrium is exclusively recorded in the oxygen isotope composition of the precipitated carbonate. Alternatively, it may simply indicate that disequilibrium is analytically better resolvable using oxygen isotopes, i.e., relative to the extent of disequilibrium, the analytical uncertainty is smaller for oxygen than for clumped isotopes.

4.5. Application to fossil material – temperature and $\delta^{18}O_{sw}$ reconstructions for the mid-Eocene

Our modern mollusc shell data provide evidence that these carbonates represent robust archives for accurate and highly precise paleotemperature reconstructions by means of exclusive Δ_{47} measurements, without the need for a mollusc-specific calibration relationship. As long as kinetic isotope effects are absent, uncertainties in reconstructed temperatures are exclusively defined by the analytical uncertainty of Δ_{47} measurements. To test whether disequilibrium effects are similarly absent in fossil material, the dual clumped isotope signature of five Eocene mollusc shells collected from the same bed were measured. All investigated fossil samples, consisting of five different species, correspond to dual clumped isotope equilibrium within the uncertainty of the measurements (Fig. 2). Δ_{47}-derived temperatures are 17.3 °C (±2.3 °C, 95CI) for FG1, 20.5 °C (±2.3 °C) for FG2, 20.3 °C (±2.3 °C) for FG3, 20.7 °C (±2.4 °C) for FM1, and 23.2 °C (±2.3 °C) for FM2 (Table 4). A temperature of 23.3 °C (±5.0 °C, 2SD) has been obtained on an older sample (42.5 Ma versus 39 Ma) from the Hampshire Basin (Evans et al., 2018), based on Δ_{47} analysis of a shallow-dwelling (symbiont-bearing) large benthic foraminifera. Marchegiano and John (2022) reported a temperature range of 15–23 °C based on Δ_{47} analysis of gastropods from the Naish Member of the Barton Clay Formation – the same member from which the samples reported here were collected. While the geologically-rapid evolution of the paleo-geography of this region in the (mid) Eocene (Clark et al., 2022; Kniest et al., 2024b) means that we cannot unambiguously ascribe the cooler mollusc versus foraminifera-derived temperatures to a changing global climate versus differences in habitat or seasonal growth patterns (although these are nonetheless within uncertainty of each other). However, we note that this is consistent with Eocene cooling globally and in the North Atlantic (Bijl et al., 2009; Inglis et al., 2015, 2023).

Insertion of Δ_{47} derived temperatures in Eq. (4) yields seawater $\delta^{18}O$ values between −3.4 ‰ and −2.2 ‰ for the mid Eocene (Table 4). These low and variable $\delta^{18}O$ seawater values agree well with those reconstructed for the Hampshire Basin, in the southern part of the North Sea, and the Paris Basin, based on a combination of $\delta^{18}O_{carb}$ and Δ_{47} data. Evans et al. (2018) analysed foraminiferal calcite from the Hampshire Basin and reported a $\delta^{18}O$ seawater value of −4.14 ‰ for an age of 42.5 Ma. Marchegiano and John (2022) analysed gastropods from the Bartonian in the Hampshire Basin and reconstructed $\delta^{18}O$ seawater values for the Naish Member of the Barton Clay Formation ranged from −1 to −2.5 ‰. Kniest et al. (2024a), analysing a 40 Ma old bivalve mollusc shell, reconstructed $\delta^{18}O$ seawater values of −0.9 ‰ to −2.7 ‰ for the Paris Basin, ascribing this substantial spatiotemporal seawater $\delta^{18}O$ variation to different degrees of freshwater input through space and time. Kniest et al. (2024b), by means of Ba/Ca and $^{87}Sr/^{86}Sr$ analysis of Eocene bivalves (genera *Venericor* and *Crassatella*), independently confirmed substantial freshwater fluxes into parts of the Hampshire Basin during the mid-Eocene. Finally, variable and negative seawater $\delta^{18}O$ values of about −2 ‰ have also been reported for the early Bartonian in the southern part of the North Sea (De Man et al., 2004). Altogether, our and these previous studies contribute to a coherent picture of relatively negative and variable seawater $\delta^{18}O$ values in this region during the mid-late Eocene. The driver of this has been suggested to be the local hydrographic regime (Kniest et al., 2024b), in particular the relatively enclosed nature of at least parts of this basin during some

intervals of the Eocene coupled with river-derived freshwater input to the relatively nearshore environments from which many of these samples derive.

5. Conclusions

We used dual clumped isotope thermometry to demonstrate that the bulk shell of molluscs may constitute a promising archive for accurate and highly precise temperature reconstructions using the Δ_{47} proxy. The majority of the specimens analysed here (15/16 modern and all fossil samples) plot indistinguishably from dual clumped isotope equilibrium, while their corresponding Δ_{47} values correspond within uncertainty to independently constrained habitat temperatures. Kinetic biases may become important at temperatures < 10 °C, but more detailed investigations are necessary to verify this hypothesis. We ascribe the absence of significant kinetic isotope effects in the clumped isotope composition to precipitation from a closely equilibrated DIC pool. Close attainment of isotopic equilibrium in the DIC pool is facilitated by the relatively low pH (~7.6–7.8) of the EPF, compared to other marine calcifiers such as corals, and utilisation of carbonic anhydrase.

In addition, we present revised empirical relationships for the temperature dependence of oxygen isotope fractionation between molluscan aragonite/calcite and water, integrating over multiple species and datasets. At relatively high temperatures, both relationships become indistinguishable from the proposed calcite-water equilibrium relationship of Coplen (2007) suggesting that calcite and aragonite may have indistinguishable states of equilibrium, but that bulk oxygen isotope equilibrium is typically not obtained at low temperatures. At these temperatures, oxygen isotopes seem to be more prone to disequilibrium effects than clumped isotopes.

Finally, we showed that a set of well-preserved Eocene mollusc samples are also characterised by equilibrium dual clumped isotope compositions. Using corresponding Δ_{47} data to reconstruct temperature and $\delta^{18}O_{sw}$ of the Hampshire Basin (UK) at ~ 39 Ma, we show that five different species are characterised by growth temperatures of 17.3–23.2 °C, all of which are within uncertainty of each other. Reconstructed seawater $\delta^{18}O$ values of −3.4 to −2.2 ‰ agree well with previous estimates, adding to a body of evidence that suggests substantial (seasonal) freshwater input to at least parts of this basin during this time.

Data availability

Data is available through Zenodo at https://doi.org/10.5281/zenodo.14961836.

CRediT authorship contribution statement

Vanessa Schlidt: Writing – review & editing, Writing – original draft, Visualization, Validation, Project administration, Methodology, Investigation, Formal analysis, Data curation, Conceptualization. **David Evans:** Writing – review & editing, Writing – original draft, Visualization, Supervision, Resources, Project administration, Methodology, Investigation, Funding acquisition, Formal analysis. **Niels J. de Winter:** Writing – review & editing, Writing – original draft, Validation, Resources, Investigation, Funding acquisition. **Miguel Bernecker:** Writing – review & editing, Software, Methodology, Investigation, Data curation. **Iris Arndt:** Writing – review & editing, Resources, Investigation. **Philip T. Staudigel:** Writing – review & editing, Investigation. **Amelia J. Davies:** Writing – review & editing, Investigation. **Uwe Brand:** Writing – review & editing, Resources. **Wolfgang Müller:** Writing – review & editing, Resources, Funding acquisition. **Jens Fiebig:** Writing – review & editing, Writing – original draft, Validation, Supervision, Resources, Project administration, Methodology, Investigation, Funding acquisition, Data curation, Conceptualization.

Declaration of competing interest

The authors declare that they have no known competing financial interests or personal relationships that could have appeared to influence the work reported in this paper.

Acknowledgments

We thank Carsten Renker and Matthias Grimm for the identification of fossil and modern species analysed in this study. Sven Hofmann, Mattia Tagliavento and Manuel Schumann are acknowledged for their support during clumped isotope analysis. Rainer Petschick kindly provided XRD measurements. Aleksandra Bitner is thanked for providing White Sea mollusc specimens, Max Janse for providing the *T. squamosa* specimen, and Rob Witbaard is thanked for providing *M. edulis* specimens. This work was enabled through FI-948/13-1 granted to JF through the Koselleck-programme of the DFG. JF, AD, DE and WM also acknowledge funding through the VeWA consortium by the LOEWE program of the Hessen Ministry of Higher Education, Research and the Arts, Germany. NJW is supported by the Dutch Science Foundation (NWO) through a VENI fellowship (Grant nr. VI. Veni.222.354) and through the FWO Climate Prize by the Flemish Research Council. DE additionally acknowledges support from the Volkswagen Stiftung Experiment! initiative (award reference: A131440). Further, WM and JF acknowledge DFG-funding through MU 3739/6-1 and FI-948/15-1, respectively.

Appendix A. Supplementary material

Supplementary Figure S1 provides a comparison of Δ_{47}/Δ_{48} values of unbleached (RG2_U), bleached RG2* and pooled RG2. Supplementary material to this article can be found online at https://doi.org/10.1016/j.gca.2025.10.008.

References

Addadi, L., Raz, S., Weiner, S., 2003. Taking advantage of disorder: amorphous calcium carbonate and its roles in biomineralization. Adv. Mater. 15, 959–970.
Addadi, L., Joester, D., Nudelman, F., Weiner, S., 2006. Mollusk shell formation: a source of new concept for understanding biomineralization process. Chem. Eur. J. 12, 980–987.
Adkins, J.F., Boyle, E.A., Curry, W.B., Lutringer, A., 2003. Stable isotopes in deep-sea corals and a new mechanism for "vital effects". Geochim. Cosmochim. Acta 67, 1129–1143.
Affek, H.P., 2013. Clumped isotopic equilibrium and the rate of isotope exchange between CO_2 and water. Am. J. Sci. 313, 309–325.
Affek, H.P., Matthews, A., Ayalon, A., Bar-Matthews, M., Burstyn, Y., Zaarur, S., Zilberman, T., 2014. Accounting for kinetic isotope effects in Soreq Cave (Israel) speleothems. Geochim. Cosmochim. Acta 143, 303–318.
Affek, H.P., Zaarur, S., 2014. Kinetic isotope effect in CO_2 degassing: insight from clumped and oxygen isotopes in laboratory precipitation experiments. Geochim. Cosmochim. Acta 143, 319–330.
Anderson, N.T., Kelson, J.R., Kele, S., Daëron, M., Bonifacie, M., Horita, J., Mackey, T.J., John, C.M., Kluge, T., Petschnig, P., Jost, A.B., Huntington, K.W., Bernasconi, S.M., Bergmann, K.D., 2021. A unified clumped isotope thermometer calibration (0.5-1,100°C) using carbonate-based standardization. Geophys. Res. Lett. 48 (7), e2020GL092069.
Arndt, I., Bernecker, M., Erhardt, T., Evans, D., Fiebig, J., Fursman, M., Kniest, J., Renema, W., Schlidt, V., Staudigel, P., Voigt, S., Müller, W., 2024. 20,000 days in the life of a giant clam reveal late Miocene tropical climate variability. Palaeogeogr. Palaeoclimatol. Palaeoecol. 661, 112711.
Bajnai, D., Fiebig, J., Tomasovych, A., Milner Garcia, S., Rollion-Bard, C., Raddatz, J., Löffler, N., Primo-Ramos, C., Brand, U., 2018. Assessing kinetic fractionation in brachiopod calcite using clumped isotopes. Sci. Rep. 8, 533.
Bajnai, D., Guo, W., Löffler, N., Methner, K., Krsnik, E., Coplen, T.B., Gischler, E., Hansen, M., Henkel, D., Price, G.D., Raddatz, J., Scholz, D., Fiebig, J., 2020. Combined clumped isotope measurements resolve kinetic biases in carbonate formation temperatures. Nat. Commun. 11, 4005.
Batenburg, S.J., Reichart, G.-J., Jilbert, T., Janse, M., Wesselingh, F.P., Renema, W., 2011. Interannual climate variability in the Miocene: high resolution trace element and stable isotope ratios in giant clams. Palaeogeogr. Palaeoclimatol. Palaeoecol. 306, 75–81.
Bernasconi, S.M., Müller, I.A., Bergmann, K.D., Breitenbach, S.F.M., Fernandez, A., Hodell, D.A., Jaggi, M., Meckler, A.N., Millan, I., Ziegler, M., 2018. Reducing

uncertainties in carbonate clumped isotope analysis through consistent carbonate-based standardization. Geochem. Geophys. Geosyst. 19 (9), 2895–2914.
Bernecker, M., Hofmann, S., Staudigel, P.T., Davies, A.J., Tagliavento, M., Meijer, N., Ballian, A., Fiebig, J., 2023. A robust methodology for triple (Δ_{47}, Δ_{48}, Δ_{49}) clumped isotope analysis of carbonates. Chem. Geol. 642, 121803.
Bernecker, M., Bonifacie, M., Staudigel, P., Meijer, N., Siebert, J., Wehr, N., Haussühl, E., Bernasconi, S.M., Petrash, D.A., Dietzel, M., Fiebig, J., 2025. Effects of mineralogy on Δ_{47} and Δ_{48} of carbonate-derived CO_2 below analytical resolution. Geochim. Cosmochim. Acta 401, 89–103.
Bertucci, A., Moya, A., Tambutté, S., Allemand, D., Supuran, C.T., Zoccola, D., 2013. Carbonic anhydrases in anthozoan corals – a review. Bioorganic Med. Chem. 21, 1437–1450.
Bijl, P.K., Schouten, S., Sluijs, A., Reichart, G.-J., Zachos, J.C., Brinkhuis, H., 2009. Early Palaeogene temperature evolution of the southwest Pacific Ocean. Nature 461, 776–779.
Burnett, L.E., 1988. Physiological responses to air exposure: acid-base balance and the role of branchial water stores. Amer. Zool. 28, 125–135.
Butler, P.G., Wanamaker, A.D., Scourse, J.D., Richardson, C.A., Reynolds, D.J., 2013. Variability of marine climate on the North Icelandic Shelf in a 1357-year proxy archive based on growth increments in the bivalve Arctica islandica. Palaeogeogr. Palaeoclimatol. Palaeoecol. 373, 141–151.
Caldarescu, D.E., Sadatzki, H., Andersson, C., Schäfer, P., Fortunato, H., Meckler, A.N., 2021. Clumped isotope thermometry in bivalve shells: a tool for reconstructing seasonal upwelling. Geochim. Cosmochim. Acta 294, 174–191.
Cardoso, J.C.R., Ferreira, V., Zhang, X., Anjos, L., Félix, R.C., Batista, F.M., Power, D.M., 2019. Evolution and diversity of alpha-carbonic anhydrases in the mantle of the Mediterranean mussel (Mytilus galloprovincialis). Sci. Rep. 9, 10400.
Carré, M., Bentaleb, I., Bruguier, O., Ordinola, E., Barrett, N.T., Fontugne, M., 2006. Calcification rate influence on trace element concentrations in aragonitic bivalve shells: evidences and mechanisms. Geochim. Cosmochim. Acta 70, 4906–4920.
Chen, S., Gagnon, A.C., Adkins, J.F., 2018. Carbonic anhydrase, coral calcification and a new model of stable isotope vital effects. Geochim. Cosmochim. Acta 236, 179–197.
Clark, A.J., Vellekoop, J., Speijer, R.P., 2022. Hydrological differences between the Lutetian Paris and Hampshire basins revealed by stable isotopes of conid gastropods. Bulletin De La Société Géologique De France 193, 3.
Coplen, T.B., 2007. Calibration of the calcite-water oxygen-isotope geothermometer at Devils Hole, Nevada, a natural laboratory. Geochim. Cosmochim. Acta 71, 3948–3957.
Crenshaw, M.A., 1972. The soluble matrix of Mercenaria mercenaria shell. Biomineralization 6, 6–11.
Curley, A.N., Petersen, S.V., Stewart, M.E., Guo, W., 2023. Biologically driven isotopic fractionations in bivalves: from paleoenvironmental problem to palaeophysiological proxy. Biol. Rev. 98, 1016–1032.
Daëron, M., Guo, W., Eiler, J., Genty, D., Blamart, D., Boch, R., Drysdale, R., Maire, R., Wainer, K., Zanchetta, G., 2011. $^{13}C^{18}O$ clumping in speleothems: observations from natural caves and precipitation experiments. Geochim. Cosmochim. Acta 75, 3303–3317.
Daëron, M., Drysdale, R.N., Peral, M., Hyughe, D., Blamart, D., Coplen, T.B., Lartaud, F., Zanchetta, G., 2019. Most Earth-surface calcites precipitate out of isotopic equilibrium. Nat. Commun. 10, 429.
Daëron, M., 2021. Full propagation of analytical uncertainties in Δ_{47} measurements. Geochem. Geophys. Geosyst. 22, 5.
Davies, A.J., John, C.M., 2019. The clumped (^{13}C-^{18}O) isotope composition of echinoid calcite: further evidence for "vital effects" in the clumped isotope proxy. Geochim. Cosmochim. Acta 245, 172–189.
Davies, A.J., Davis, S., John, C.M., 2021. Evidence of taxonomic non-equilibrium effects in the clumped isotope composition of modern cephalopod carbonate. Chem. Geol. 578, 120317.
Davies, A.J., Guo, W., Bernecker, M., Tagliavento, M., Raddatz, J., Gischler, E., Flögel, S., Fiebig, J., 2022. Dual clumped isotope thermometry of coral carbonate. Geochim. Cosmochim. Acta 338, 66–78.
Davies, A.J., Brand, U., Tagliavento, M., Bitner, M.A., Bajnai, D., Staudigel, P.T., Bernecker, M., Fiebig, J., 2023. Isotopic disequilibrium in brachiopods disentangled with dual clumped isotope thermometry. Geochim. Cosmochim. Acta 359, 135–147.
Defliese, W.F., Hren, M.T., Lohmann, K.C., 2015. Compositional and temperature effects of phosphoric acid fractionation on Δ_{47} analysis and implications for discrepant calibrations. Chem. Geol. 396, 51–60.
De Man, E., Ivany, L., Vandenberghe, N., 2004. Stable oxygen isotope record of the eocene-oligocene transition in the southern North Sea Basin: positioning the Oi-1 event. Netherlands J. Geosci. / Geologie En Mijnbouw 83, 193–197.
Dennis, K.J., Affek, H.P., Passey, B.H., Schrag, D.P., Eiler, J.M., 2011. Defining an absolute reference frame for 'clumped' isotope studies of CO_2. Geochim. Cosmochim. Acta 75, 7117–7131.
de Winter, N.J., Vellekoop, J., Clark, A.J., Stassen, P., Speijer, R., Claeys, P., 2020. The giant marine gastropod Campanile giganteum (Lamarck, 1804) as a high-resolution archive of seasonality in the Eocene greenhouse world. Geochem., Geophys., Geosyst. 21 (4), e2019GC008794.
de Winter, N.J., Dämmer, L.K., Falkenroth, M., Reichart, G.-J., Moretti, S., Martínez-García, A., Höche, N., Schöne, B.R., Rodiouchkina, K., Goderis, S., Vanhaecke, F., van Leeuwen, S.M., Ziegler, M., 2021a. Multi-isotopic and trace element evidence against different formation pathways for oyster microstructures. Geochim. Cosmochim. Acta 308, 326–352.
de Winter, N.J., Agterhuis, T., Ziegler, M., 2021b. Optimizing sampling strategies in high-resolution paleoclimate records. Climate of the Past 17, 1315–1340.
de Winter, N.J., Witbaard, R., Kocken, I.J., Müller, I.A., Guo, J., Goudsmit, B., Ziegler, M., 2022. Temperature dependence of clumped isotopes (Δ_{47}) in aragonite. Geophys. Res. Lett. 49, e2022GL099479.
Dietzel, M., Tang, J., Leis, A., Köhler, S.J., 2009. Oxygen isotopic fractionation during inorganic calcite precipitation – effects of temperature, precipitation rate and pH. Chem. Geol. 268, 107–115.
Evans, D., Sagoo, N., Renema, W., Cotton, L.J., Müller, W., Todd, J.A., Saraswati, P.K., Stassen, P., Ziegler, M., Pearson, P.N., Valdes, P.J., Affek, H.P., 2018. Eocene greenhouse climate revealed by coupled clumped isotope-Mg/Ca thermometry. Proc. Natl. Acad. Sci. USA 115, 1174–1179.
Fiebig, J., Bajnai, D., Löffler, N., Methner, K., Krsnik, E., Mulch, A., Hofmann, S., 2019. Combined high-precision Δ_{48} and Δ_{47} analysis of carbonate. Chem. Geol. 522, 186–191.
Fiebig, J., Daeron, M., Bernecker, M., Guo, W., Schneider, G., Boch, R., Bernasconi, S.M., Jautzy, J., Dietzel, M., 2021. Calibration of the dual clumped isotope thermometer for carbonates. Geochim. Cosmochim. Acta 312, 235–256.
Fiebig, J., Bernecker, M., Meijer, N., Methner, K., Staudigel, P.T., Davies, A.J., Bayarjargal, L., Spahr, D., Winkler, B., Hofmann, S., Granzin, M., Petersen, S.V., 2024. Carbonate clumped isotope values compromised by nitrate-derived NO_2 interferent. Chem. Geol. 670, 122382.
Fitzer, S.C., Chung, P., Maccherozzi, F., Dhesi, S.S., Kamensos, N.A., Phoenix, V.R., Cusack, M., 2016. Biomineral shell formation under ocean acidification: a shift from order to chaos. Sci. Rep. 6, 21076.
Freeman, J.A., Willbur, K.M., 1948. Carbonic anhydrase in molluscs. Biol. Bull. 94, 55–59.
Ghosh, P., Adkins, J., Affek, H., Balta, B., Guo, W., Schauble, E.A., Schrag, D., Eiler, J.M., 2006. ^{13}C-^{18}O bonds in carbonate minerals: a new kind of paleothermometer. Geochim. Cosmochim. Acta 70, 1439–1456.
Goodwin, D.H., Flessa, K.W., Schöne, B.R., Dettman, D.L., 2001. Cross-calibration of daily growth increments, stable isotope variation, and temperature in the Gulf of California bivalve mollusk Chione cortezi: implications for paleoenvironmental analysis. PALAIOS 16, 387–398.
Grossman, E.L., Ku, T.-L., 1986. Oxygen and carbon isotope fractionation in biogenic aragonite: temperature effects. Chem. Geol. 59, 59–74.
Guo, W., 2020. Kinetic clumped isotope fractionation in the DIC-H_2O-CO_2 system: patterns, controls, and implications. Geochim. Cosmochim. Acta 268, 230–257.
Guo, W., Zhou, C., 2019. Patterns and controls of disequilibrium isotope effects in speleothems: insights from an isotope-enabled diffusion-reaction model and implications for quantitative thermometry. Geochim. Cosmochim. Acta 267, 196–226.
Harwood, A.J.P., Dennis, P.F., Marca, A.D., Pilling, G.M., Millner, R.S., 2008. The oxygen isotope composition of water masses within the North Sea. Estuar. Coast. Shelf Sci. 78, 353–359.
Henkes, G.A., Passey, B.H., Wanamaker Jr., A.D., Grossman, E.L., Ambrose Jr., W.G., Carroll, M.L., 2013. Carbonate clumped isotope compositions of modern marine mollusc and brachiopod shells. Geochim. Cosmochim. Acta 106, 307–325.
Hill, P.S., Tripati, A.K., Schauble, E.A., 2014. Theoretical constraints on the effects of pH, salinity, and temperature on clumped isotope signatures of dissolved inorganic carbon species and precipitating carbonate minerals. Geochim. Cosmochim. Acta 125, 610–651.
Huyghe, D., Lartaud, F., Emmanuel, L., Merle, D., Renard, M., 2015. Palaeogene climate evolution in the Paris Basin from oxygen stable isotope ($\delta^{18}O$) compositions of marine molluscs. J. Geol. Soc. London 172, 576–587.
Huyghe, D., Daeron, M., de Rafelis, M., Blamart, D., Sébilo, M., Paulet, Y.-M., Lartaud, F., 2022. Clumped isotopes in modern marine bivalves. Geochim. Cosmochim. Acta 316, 41–58.
Immenhauser, A., Schöne, B.R., Hoffmann, R., Niedermayr, A., 2016. Mollusc and brachiopod skeletal hard parts: Intricate archives of their marine environment. Sedimentology 63, 1–59.
Ingalls, M., Leapaldt, H.C., Lloyd, M.K., 2024. Microbial autotrophy recorded by carbonate dual clumped isotope disequilibrium. Geochem. Geophys. Geosyst. 25, e2024GC011590.
Inglis, G.N., Farnsworth, A., Lunt, D., Foster, G.L., Hollis, C.J., Pagani, M., Jardine, P.E., Pearson, P.N., Markwick, P., Galsworthy, A.M.J., Raynham, L., Taylor, K.W.R., Pancost, R.D., 2015. Descent toward the Icehouse: eocene sea surface cooling inferred from GDGT distributions. Paleoceanography 30, 1000–1020.
Inglis, G.M., Bhatia, R., Evans, D., Zhu, J., Müller, W., Mattey, D., Thornalley, D.J.R., Stockey, R.G., Wade, B.S., 2023. Surface ocean cooling in the Eocene North Atlantic coincides with declining atmospheric CO_2. Geophys. Res. Lett. 50 (24) e2023GL105448.
Ip, Y.K., Loong, A.M., Hiong, K.C., Wong, W.P., Chew, S.F., Reddy, K., Sivaloganathan, B., Ballantyne, J.S., 2006. Light induces an increase in the pH of and a decrease in the ammonia concentration in the extrapallial fluid of the giant clam Tridacna squamosa. Physiol. Biochem. Zool. 79, 656–664.
Ivany, L.C., Judd, E.J., 2022. Deciphering temperature seasonality in earth's ancient oceans. Annu. Rev. Earth Planet. Sci. 50, 123–152.
Jacob, D.E., Wirth, R., Soldati, A.L., Wehrmeister, U., Schreiber, A., 2011. Amorphous calcium carbonate in the shells of adult *Unionoida*. J. Struct. Biol. 173 (2), 241–249.
Janse, M., Wensing, J., Gieling, H., de Jongh, T., Leewis, R., 2008. Ecological management of a large coral reef eco-display at Burgers' Zoo, Arnhem, The Netherlands. in: Advances in Coral Husbandry in Public Aquariums Public Aquarium Husbandry Series, eds RJ Leewis and M. Janse (Arnhem: Burgers' Zoo), pp.293-303.
Jansen, J.M., Pronker, A.E., Kube, S., Sokolowski, A., Sola, J.C., Marquiegui, M.A., Schiedek, D., Bonga, S.W., Wolowicz, M., Hummel, H., 2007. Geographic and seasonal patterns and limits on the adaptive response to temperature of European *Mytilus* spp. and *Macoma balthica* populations. Oecologia 154, 23–34.

Jautzy, J., Savard, M., Dhillon, R., Bernasconi, S., Lavoie, D., Smirnoff, A., 2020. Clumped isotope temperature calibration for calcite: Bridging theory and experimentation. Geochem. Perspect. Lett. 14, 36–41.
Judd, E.J., Wilkinson, B.H., Ivany, L.C., 2017. The life and time of clams: derivation of intra-annual growth rates from high-resolution oxygen isotope profiles. Palaeogeogr. Palaeoclimatol. Palaeoecol. 490, 70–83.
Judd, E.J., Tierney, J.E., Lunt, D.J., Montañez, I.P., Huber, B.T., Wing, S.L., Valdes, P.J., 2024. A 485-million-year history of Earth's surface temperature. Science 385, eadk3705.
Kaandorp, R.J.G., Vonhof, H.B., Del Busto, C., Wesselingh, F.P., Ganssen, G.M., Marmól, A.E., Romero Pittman, L., van Hinte, J.E., 2003. Seasonal stable isotope variations of the modern Amazonian freshwater bivalve *Anodontites trapesialis*. Palaeogeogr. Palaeoclimatol. Palaeoecol. 194, 339–354.
Kelson, J.R., Huntington, K.W., Schauer, A.J., Saenger, C., Lechler, A.R., 2017. Toward a universal carbonate clumped isotope calibration: diverse synthesis and preparatory methods suggest a single temperature relationship. Geochim. Cosmochim. Acta 197, 104–131.
Kim, S.-T., O'Neil, J.R., 1997. Equilibrium and nonequilibrium oxygen isotope effects in synthetic carbonates. Geochim. Cosmochim. Acta 61, 3461–3475.
Kim, S.-T., Mucci, A., Taylor, B.E., 2007a. Phosphoric acid fractionation factors for calcite and aragonite between 25 and 75°C: revisited. Chem. Geol. 246, 135–146.
Kim, S.-T., O'Neil, J.R., Hillaire-Marcel, C., Mucci, A., 2007b. Oxygen isotope fractionation between synthetic aragonite and water: influence of temperature and Mg^{2+} concentration. Geochim. Cosmochim. Acta 71, 4704–4715.
Kniest, J.F., Davies, A.J., Brugger, J., Fiebig, J., Bernecker, M., Todd, J.A., Hickler, T., Voigt, S., Woodland, A., Raddatz, J., 2024a. Dual clumped isotopes from the Mid-Eocene bivalve shell reveal a hot and summer wet climate of the Paris Basin. Commun. Earth Environ. 5, 330.
Kniest, J.F., Evans, D., Gerdes, A., Cantine, M., Todd, J.A., Sigwart, J.D., Vellekoop, J., Müller, W., Voigt, S., Raddatz, J., 2024b. Spatiotemporal changes in riverine input into the Eocene North Sea revealed by strontium isotope and barium analysis of bivalve shells. Sci. Rep. 14, 28806.
Lécuyer, C., Hutzler, A., Amiot, R., Daux, V., Grosheny, D., Otero, O., Martineau, F., Fourel, F., Balter, V., Reynard, B., 2012. Carbon and oxygen isotope fractionations between aragonite and calcite of shells from modern molluscs. Chem. Geol. 332–333, 92–101.
Lécuyer, C., Reynard, B., Martineau, F., 2004. Stable isotope fractionation between mollusc shells and marine waters from Martinique Island. Chem. Geol. 213, 293–305.
Le Roy, N., Jackson, D.J., Marie, B., Ramos-Silva, P., Marin, F., 2016. Carbonic anhydrase and metazoan biocalcification: a focus on molluscs. Key Eng. Mater. 672 (151), 157.
Levitt, N.P., Eiler, J.M., Romanek, C.S., Beard, B.L., Xu, H., Johnson, C.M., 2018. Near equilibrium ^{13}C-^{18}O bonding during inorganic calcite precipitation under chemostat conditions. Geochem. Geophys. Geosyst. 19, 901–920.
Lindinger, M.I., Lauren, D.J., McDonald, D.G., 1984. Acid-base-balance in the sea mussel, Mytilus edulis. 3. Effects of environmental hypercapnia on intracellular and extracellular acid-base-balance. Marine Bio. Lett. 5, 371–381.
Locarnini, R.A., Mishonov, A.V., Baranova, O.K., Reagan, J.R., Boyer, T.P., Seidov, D., Wang, Z., Garcia, H.E., Bouchard, C., Cross, S.L., Paver, C.R., and Dukhovskoy, D. (2024). World Ocean Atlas 2023, Volume 1: Temperature. A. Mishonov, Technical Editor, NOAA Atlas NESDIS 89, doi.org/10.25923/54bh-1613.
Lu, C., Murray, S.T., Klaus, J., McNeill, D.F., Swart, P.K., 2024. Dual clumped isotopes ((Δ_{47} and Δ_{48}) reveal non-equilibrium formation of freshwater cements. Geochim. Cosmochim. Acta 379, 145–157.
Lu, C.L., Swart, P.K., 2024. The application of dual clumped isotope thermometer ((Δ_{47} and Δ_{48}) to the understanding of dolomite formation. Geology 52, 56–60.
Marchegiano, M., John, C.M., 2022. Disentangling the impact of global and regional climate changes during the Middle Eocene in the Hampshire Basin: New insights from carbonate clumped isotopes and ostracod assemblages. Paleoceanogr. Paleoclimatol. 37, e2021PA004299.
Marie, B., Luquet, G., Bédouet, L., Milet, C., Guichard, N., Medakovic, D., Marin, F., 2008. Nacre Calcification in the Freshwater Mussel *Unio pictorium*: Carbonic Anhydrase activity and Purificaion of a 95 kDa Calcium-Binding Glycoprotein. Chembiochem 9, 2515–2523.
McConnaughey, T., 1989a. ^{13}C and ^{18}O disequilibrium in biological carbonates: I. Patterns. Geochimica et Cosmochimica Acta 53, 151–162.
McConnaughey, T., 1989b. ^{13}C and ^{18}O isotopic disequilibrium in biological carbonates: II. *In vitro* simulation of kinetic isotope effects. Geochim. Cosmochim. Acta 53, 163–171.
Miyamoto, H., Miyashita, T., Okushima, M., Nakano, S., Morita, T., Matsushiro, A., 1996. A carbonic anhydrase from the nacreous layer in oyster pearls. Proc. Natl. Acad. Sci. USA 93, 9657–9660.
Miyamoto, H., Miyoshi, F., Kohno, J., 2005. The carbonic anhydrase domain protein nacrein is expressed in the epithelial cells of the mantle and acts as a negative regulator in calcification in the mollusk Pinctada fucata. Zoolog. Sci. 22, 311–315.
Nassif, N., Pinna, N., Gehrke, N., Antonietti, M., Jäger, C., Cölfen, H., 2005. Amorphous layer around aragonite platelets in nacre. Proc. Natl. Acad. Sci. USA 102 (36), 12653–12655.
Nehrke, G., Poigner, H., Wilhelms-Dick, D., Brey, T., Abele, D., 2012. Coexistencew of three calcium carbonate polymorphs in the shell of the Antarctic clam Laternula elliptica. Geochem. Geophys. Geosyst. 13, 5.
Nielsen, S.A., Frieden, E., 1972. Carbonic anhydrase activity in molluscs. Comp. Biochem. Physiol. 41B, 461–468.
Nooitgedacht, C.W., van der Lubbe, H.J.L., Ziegler, M., Staudigel, P.T., 2021. Internal water facilitates thermal resetting of clumped isotopes in biogenic aragonite. Geochem. Geophys. Geosyst. 22, e2021GC009730.
Park, D.-K., Lee, M.S., 2019. Kinetic study of catalytic CO_2 hydration by metal-substituted biomimetic carbonic anhydrase model complexes. R. Soc. Open Sci. 6, 190407.
Parvez, Z.A., Lucarelli, J.K., Matamaros, I.W., Rubi, J., Miguel, K., Elliott, B., Flores, R., Ulrich, R.N., Eagle, R.A., Watkins, J.M., Christensen, J.N., Tripati, A., 2023. Dual carbonate clumped isotopes (Δ_{47}-Δ_{48}) constrains kinetic effects and timescales in peridotite-associated springs at the Cedars, Northern California. Geochim. Cosmochim. Acta 358, 77–92.
Parvez, Z.A., El-Shenawy, M., Lucarelli, J.K., Kim, S.T., Johnson, K.R., Wright, K., Gebregiorgis, D., Montanez, I.P., Wortham, B., Asrat, A., Reinhardt, E., Christensen, J.N., Matamoros, I.W., Rubi, J., Miguel, K., Elliott, B.M., Flores, R., Kovacs, S., Eagle, R.A., Tripati, A., 2024. Dual carbonate clumped isotope ((Δ_{47}-Δ_{48}) measurements constrain different sources of kinetic isotope effects and quasi-equilibrium signatures in cave carbonates. Geochim. Cosmochim. Acta 366, 95–112.
Payne, J.L., Heim, N.A., Knope, M.L., McClain, C.R., 2014. Metabolic dominance of bivalves predates brachiopod diversity decline by more than 150 million years. Proc. R. Soc. B 281, 20133122.
Pederson, C., Mavromatis, V., Dietzel, M., Rollion-Bard, C., Nehrke, G., Jöns, N., Jochum, K.P., Immenhauser, A., 2019. Diagenesis of mollusc aragonite and the role of fluid reservoirs. Earth Planet. Sci. Lett. 514, 130–142.
Ross, C.L., Warnes, A., Comeau, S., Cornwall, C.E., Cuttler, M.V.W., Naugle, M., McCulloch, M.T., Schoepf, V., 2022. Coral calcification mechanisms in a warming ocean and the interactive effects of temperature and light. Commun. Earth Environ. 3, 72.
Sade, Z., Halevy, I., 2017. New constraints on kinetic isotope effects during CO_2(aq) hydration and hydroxylation: revisiting theoretical and experimental data. Geochimica et Cosmochimica 214, 246–265.
Saenger, C., Affek, H.P., Felis, T., Thiagarajan, N., Lough, J.M., Holcomb, M., 2012. Carbonate clumped isotope variability in shallow water corals: temperature dependence and growth-related vital effects. Geochim. Cosmochim. Acta 99, 224–242.
Saenger, C., Gabitov, R.I., Farmer, J., Watkins, J.M., Stone, R., 2017. Linear correlations in bamboo coral $\delta^{13}C$ and $\delta^{18}O$ sampled by SIMS and micromill: evaluating paleoceanographic potential and biomineralization mechanisms using $\delta^{11}B$ and Δ_{47} composition. Chem. Geol. 454, 1–14.
Schauble, E.A., Ghosh, P., Eiler, J.M., 2006. Preferential formation of ^{13}C-^{18}O bonds in carbonate minerals, estimated using first-principles lattice dynamics. Geochim. Cosmochim. Acta 70, 2510–2529.
Schmidt, G.A., G. R. Bigg and E. J. Rohling. 1999. "Global Seawater Oxygen-18 Database - v1.22" https://data.giss.nasa.gov/o18data/.
Schöne, B.R., Fiebig, J., Pfeiffer, M., Gleβ, R., Hickson, J., Johnson, A.L., Dreyer, W., Oschmann, W., 2005. Climate records from a bivalved Methuselah (*Arctica islandica*, Mollusca; Iceland). Palaeogeography, Palaeoclimatol., Palaeoecol. 228, 130–148.
Spooner, P.T., Guo, W., Robinson, L.F., Thiagarajan, N., Hendry, K.R., Rosenheim, B.E., Leng, M.J., 2016. Clumped isotope composition of cold-water corals: a role for vital effects? Geochimica et Cosmochimica Acta 179, 123–141.
Staudigel, P.T., Pederson, C., van der Lubbe, J., Bernecker, M., Tagliavento, M., Davies, A.J., Immenhauser, A., Fiebig, J., 2023a. An isotopologue-enabled model (Δ_{47}, Δ_{48}) for describing thermal fluid-carbonate interaction in open and closed diagenetic systems. Geochem., Geophys., Geosyst. 24, e2023GC011117.
Staudigel, P., Davies, A.J., Bernecker, M., Tagliavento, M., van der Lubbe, H.J.L., Nooitgedacht, C., Looser, N., Bernasconi, S.M., Vonhof, H., Price, G., Fiebig, J., 2023b. Fingerprinting kinetic isotope effects and diagenetic exchange reactions using fluid inclusion and dual-clumped isotope analysis. Geochem., Geophys., Geosyst. 24, e2022GC010766.
Staudigel, P.T., Feng, D., Peckmann, J., Bernecker, M., Davies, A.J., Tagliavento, M., Fiebig, J., 2024. Resolving and correcting for kinetic biases on methane seep paleotemperature using carbonate Δ_{47}/Δ_{48} analysis. Sci. Adv. 10, eadn0155.
Swart, P.K., Lu, C., Moore, E.W., Smith, M.E., Murray, S.T., Staudigel, P.T., 2021. A calibration equation between Δ_{48} values of carbonate and temperature. Rap. Commun. Mass Spectrom. 35, e9147.
Tagliarolo, M., Grall, J., Chavaud, L., Clavier, J., 2013a. Aerial and underwater metabolism of Patella vulgata L.: comparison of three intertidal levels. Hydrobiologia 702, 241–253.
Tagliarolo, M., Clavier, J., Chauvaud, L., Grall, J., 2013b. Carbon emission associated with respiration and calcification of nine gastropod species from the intertidal rocky shore of Western Europe. Marine Biology 160, 2891–2901.
Tagliavento, M., Davies, A.J., Bernecker, M., Staudigel, P.T., Dawson, R.R., Dietzel, M., Götschl, K., Guo, W., Schulp, A.S., Therrien, F., Zelenitsky, D.K., Gerdes, A., Müller, W., Fiebig, J., 2023. Evidence for heterothermic endothermy and reptile-like eggshell mineralization in Troodon, a non-avian maniraptoran theropod. Proc. Natl. Acad. Sci. USA 120, e2213987120.
Thiagarajan, N., Adkins, J., Eiler, J., 2011. Carbonate clumped isotope thermometry of deep-sea corals and implications for vital effects. Geochimica et Cosmochimica Acta 75, 4416–4425.
Tripati, A.K., Hill, P.S., Eagle, R.A., Mosenfelder, J.L., Tang, J., Schauble, E.A., Eiler, J. M., Zeebe, R.E., Uchikawa, J., Coplen, T.B., Ries, J.B., Henry, D., 2015. Beyond temperature: clumped isotope signatures in dissolved inorganic carbon species and the influence of solution chemistry on carbonate mineral composition. Geochimica et Cosmochimica Acta 166, 344–371.
Uchikawa, J., Zeebe, R.E., 2012. The effect of carbonic anhydrase on the kinetics and equilibrium of the oxygen isotope exchange in the CO_2-H_2O system: implications for $\delta^{18}O$ vital effects in biogenic carbonates. Geochimica et Cosmochimica Acta 95, 15–34.

Venn, A.A., Tambutté, E., Caminti-Segonds, N., Techer, N., Allemand, D., Tambutté, S., 2019. Effects of light and darkness on pH ragulation in three coral species exposed to seawater acidification. Scientific Reports 9, 2201.
Vihtakari, M., Renaud, P.E., Clarke, L.J., Whitehouse, M.J., Hop, H., Carroll, M.L., Ambrose Jr, W.G., 2016. Decoding the oxygen isotope signal for seasonal growth patterns in Arctic bivalves. Palaeogeography, Palaeoclimatology, Palaeoecology 446, 263–283.
Wang, Z., Gaetani, G., Liu, C., Cohen, A., 2013. Oxygen isotope fractionation between aragonite and seawater: developing a novel kinetic oxygen isotope fractionation model. Geochimica et Cosmochimica Acta 117, 232–251.
Watkins, J.M., Nielsen, L.C., Ryerson, F.J., Paolo, D.J., 2013. The influence of kinetics on the oxygen isotope composition of calcium carbonate. Earth Planet. Sci. Lett. 375, 349–360.
Watkins, J.M., Hunt, J.D., Ryerson, F.J., Paolo, D.J., 2014. The influence of temperature, pH, and growth rate on the $\delta^{18}O$ composition of inorganically precipitated calcite. Earth Planet. Sci. Lett. 404, 332–343.
Weber, J.N., Woodhead, P.M.J., 1972. Temperature dependence of oxygen-18 concentration in reef coral carbonates. J. Geophys. Res. 77, 463–473.
Weiss, I.M., Tuross, N., Addadi, L., Weiner, S., 2002. Mollusc larval shell formation: amorphous calcium carbonate is a precursor phase for aragonite. J. Exp. Zoo. 293, 478–491.
White, J.H., Defliese, W.F., 2023. $\delta^{13}C$ and $\delta^{18}O$ heterogeneities in carbonates: nonlinear mixing in the application of dual-carbonate-clumped isotope thermometer. Rapid Commun. Mass Spectrometry 37, e9627.
Witbaard, R., Jenness, M.I., Van Der Borg, K., Ganssen, G., 1994. Verification of annual growth increments in Arctica islandica L. from the North Sea by means of oxygen and carbon isotopes. Netherlands J. Sea Res. 33, 91–101.